The SO(5) Deconfined Phase Transition under the Fuzzy Sphere Microscope: Approximate Conformal Symmetry, Pseudo-Criticality, and Operator Spectrum

Zheng Zhou (周正),[1, 2] Liangdong Hu,[3] W. Zhu,[3] and Yin-Chen He[1]

[1]*Perimeter Institute for Theoretical Physics, Waterloo, Ontario N2L 2Y5, Canada*
[2]*Department of Physics and Astronomy, University of Waterloo, Waterloo, Ontario N2L 3G1, Canada*
[3]*Westlake Institute of Advanced Study, Westlake University, Hangzhou 310024, China*

The deconfined quantum critical point (DQCP) is an example of phase transitions beyond the Landau symmetry breaking paradigm that attracts wide interest. However, its nature has not been settled after decades of study. In this paper, we apply the recently proposed fuzzy sphere regularization to study the SO(5) non-linear sigma model (NLσM) with a topological Wess-Zumino-Witten term, which serves as a dual description of the DQCP with an exact SO(5) symmetry. We demonstrate that the fuzzy sphere functions as a powerful microscope, magnifying and revealing a wealth of crucial information about the DQCP, ultimately paving the way towards its final answer. In particular, through exact diagonalization, we provide clear evidence that the DQCP exhibits approximate conformal symmetry. The evidence includes the existence of a conserved SO(5) symmetry current, a stress tensor, and integer-spaced levels between conformal primaries and their descendants. Most remarkably, we have identified 19 conformal primaries and their 82 descendants. Furthermore, by examining the renormalization group flow of the lowest symmetry singlet, we demonstrate that the DQCP is more likely pseudo-critical, with the approximate conformal symmetry plausibly emerging from nearby complex fixed points. Our computed primary spectrum also has important implications, including the conclusion that the SO(5) DQCP cannot describe a direct transition from the Néel to valence bond solid phase on the honeycomb lattice.

I. INTRODUCTION

The study of universal properties of quantum phase transitions has been a central task within the condensed matter physics community [1]. While Landau's spontaneous symmetry breaking paradigm has provided insights into many criticalities, researchers have also identified exotic quantum phase transitions that defy this paradigm. One famous example is the deconfined quantum critical point (DQCP) [2, 3], initially proposed to describe a direct quantum phase transition between the Néel anti-ferromagnet (AFM) and the valence bond solid (VBS) on a square lattice [4–6]. DQCP, besides being one of the pioneering phase transitions beyond Landau symmetry breaking, has led to numerous theoretical surprises, including the emergence of SO(5) symmetry [7] and the conjectural duality between different strongly interacting 3D (i.e., (2 + 1)D) gauge theories [8].

Since its proposal, DQCP has undergone extensive studies in various models over the past two decades [7, 9–30] (also see a recent review [31]). However, its nature remains controversial. Monte Carlo simulations of DQCP in different models have shown no signals of discontinuity, thus suggesting a continuous phase transition. However, abnormal scaling behaviors have been observed [7, 22]. Moreover, the critical exponents obtained by Monte Carlo simulations violate the rigorous bounds from the conformal bootstrap method [32, 33]. Several possibilities have been proposed to reconcile these tensions. One possibility is that DQCP represents a continuous quantum phase transition that does not exhibit emergent conformal symmetry. Alternatively, it is possible that previous Monte Carlo analyses failed to obtain precise critical exponents due to the presence of abnormal scaling behavior [14, 19, 22, 25]. Among these possibilities, a particularly intriguing proposal is the concept of pseudo-criticality [8], also known as walking behavior caused by a complex fixed point [34, 35]. According to this proposal, DQCP manifests as a weakly first-order tran-

sition with a tiny gap and a large correlation length. In contrast to conventional first-order phase transitions, a pseudo-critical system demonstrates behavior closely resembling a continuous transition, adhering to universal behaviors, especially at energy scales (e.g., finite temperature in real experiments) larger than its small energy gap.

Theoretically, a pseudo-critical system resides near complex fixed points within the unphysical (non-unitary) parameter space. Under the renormalization group (RG) flow, the system slowly walks in the shadow of complex fixed points, resulting in approximate scaling and conformal symmetry [8, 34, 35]. A notable example of pseudo-criticality is observed in a famous weakly first-order transition, i.e., the order-disorder transition of the 2D ((1 + 1)D) 5-state Potts model [36]. Numerical investigations have indeed revealed approximate conformal symmetry in this model [37]. However, despite the plausibility of pseudo-criticality as a scenario consistent with most numerical findings regarding DQCP [38, 39], direct evidence remains elusive.

In general, understanding 3D interacting phase transitions such as DQCP requires non-perturbative tools like numerical methods. Historically, Monte Carlo simulation of lattice models has been the primary reliable numerical method for studying 3D phase transitions. However, this approach faces several challenges when tackling problems like DQCP. Firstly, Monte Carlo simulations do not provide direct information regarding the emergent conformal symmetry. Secondly, they heavily rely on finite-size extrapolation of physical observables such as correlators to extract critical exponents, limiting access to only a small number of critical exponents. Moreover, subtle issues may arise if there is abnormal scaling behavior in the pseudo-critical system. Lastly, the similarity in behavior between pseudo-critical and true critical systems makes it exceedingly difficult to distinguish them, despite a few proposals [40, 41] that currently lack a well-founded theoretical foundation.

A novel approach, called fuzzy sphere regularization, has recently emerged as a powerful method for studying critical phenomena in 3D (i.e., $(2 + 1)$D) [42]. It involves investigating the $(2 + 1)$D quantum phase transition on the geometry of $S^2 \times \mathbb{R}$ using the fuzzy (non-commutative) sphere [43]. This approach offers distinct advantages over traditional lattice model-based methods, including the direct observation of emergent conformal symmetry and the efficient extraction of critical data, such as critical exponents, by employing the state-operator correspondence, without relying on finite-size extrapolation. A key feature of the fuzzy sphere scheme is the state-operator correspondence [44, 45], which allows easy access to information such as the scaling dimensions of many operators. Specifically, there is a one-to-one correspondence between the eigenstates $|k\rangle$ of the CFT quantum Hamiltonians on the sphere and the CFT operators. Moreover, the energy gaps δE_k are proportional to the scaling dimensions Δ_k of the CFT operators

$$\delta E_k = E_k - E_0 = \text{constant} \times \Delta_k, \tag{1}$$

where the scale factor is model and size dependent. The power of this approach has been demonstrated in the context of the 3D Ising transition, where the presence of emergent conformal symmetry has been convincingly established [42]. Moreover, accurate and efficient determinations of 15 primary operators (i.e., independent critical exponents) [42], 13 operator product expansion (OPE) coefficients [46], and several four-point correlators [47] have been achieved as well. Therefore, the fuzzy sphere can serve as a powerful microscope for studying 3D critical phenomena, magnifying and revealing crucial information that is inaccessible through other approaches.

In this paper, using the fuzzy sphere microscope, we provide direct evidence that the SO(5) DQCP is pseudo-critical with an approximate conformal symmetry. Specifically, we investigate the 3D SO(5) non-linear sigma model (NLσM) with a level-1 Wess-Zumino-Witten (WZW) term, which serves as one of the dual descriptions of the SO(5) DQCP [7, 8]. A similar model has been previously studied on the torus using determinant Monte Carlo methods [30, 48]. Throughout a wide range of interaction strengths, we observe an approximate conformal symmetry in the excitation spectrum of the Hamiltonian, confirmed by the identification of the conserved SO(5) symmetry current, stress tensor, and the (approximately) integer-spaced levels between various conformal primaries and their descendants. Interestingly, as we vary the system size, we find that the renormalization group (RG) flow is consistent with pseudo-criticality. In particular, we observe the lowest symmetry singlet flowing from being slightly irrelevant to slightly relevant, which is a characteristic feature of pseudo-criticality. Furthermore, we identify and calculate the scaling dimensions of various primary operators in the operator spectrum, some of which are crucial for understanding the physics of the DQCP. For instance, our estimated critical exponent η for the SO(5) order parameter is consistent with previous Monte Carlo estimations. Additionally, we find that the lowest parity-odd SO(5) singlet is highly irrelevant with a scaling dimension of approximately $\Delta \approx 5.4$. If this operator were relevant, it would drive the DQCP towards a chiral spin liquid, poten-

tially playing a role in interesting phenomena observed in real materials [49]. We also identify a relevant 6π-monopole (in the language of the CP^1 model), indicating that the Néel-VBS transition on the honeycomb lattice cannot be described by the SO(5) DQCP [21]. Conversely, the 8π-monopole is found to be irrelevant, supporting the original conjecture of a stable DQCP on the square lattice.

The paper is organized as follows. In Sec. II A, we explain the Hamiltonian of the non-linear sigma model on the lowest Landau level and fuzzy sphere. We then discuss the possible scenarios of the RG flow, in particular, the conformal window and pseudo-criticality, in Sec. II B; following that, in Sec. II C, we discuss the relation with the original Néel-VBS DQCP. We then present our numerical results in Sec. III. In particular, we provide strong evidence for approximate conformal symmetry and support the scenario of pseudo-criticality in Sec. III C; in Sec. III D, we discuss the operator spectrum and its physical consequence; in Sec. III E, we calculate the correlation functions and OPE coefficients. Finally, we present a summary and discussion in Sec. IV. The appendices contain more discussion about the formalism and detailed numerical data of the spectra.

II. DECONFINED PHASE TRANSITION ON THE FUZZY SPHERE

A. Model

The deconfined quantum critical point (DQCP) has multiple dual theoretical descriptions [8], one of which involves the 3D SO(5) non-linear sigma model (NLσM) with a level-1 Wess-Zumino-Witten (WZW) term [7]. It has been found that this SO(5) NLσM can be naturally realized with electrons in the half-filled lowest Landau level (LLL), where an intriguing aspect is that the UV Hamiltonian has an exact SO(5) symmetry [30, 48]. Our fuzzy sphere model is a spherical realization of this proposal, albeit formulated in a slightly different form.

The target space of the SO(5) NLσM is $S^4 \cong \frac{\text{SO}(5)}{\text{SO}(4)} \cong \frac{\text{Sp}(2)}{\text{Sp}(1)\times\text{Sp}(1)}$. Here, we adopt the convention that $\text{Sp}(1) \cong \text{SU}(2)$ and $\text{Sp}(2) \cong \text{Spin}(5)$ (where $\text{Spin}(5)$ is the double cover of SO(5)). Although we will only study the SO(5) NLσM numerically in this paper, it is highly beneficial to consider its large-N generalization, namely the $\text{Sp}(2N)$ Grassmannian NLσM defined on the target space $\frac{\text{Sp}(2N)}{\text{Sp}(N)\times\text{Sp}(N)}$. Interestingly, this $\text{Sp}(2N)$ Grassmannian NLσM can also be straightforwardly realized using LLL.

We begin with $4N$-flavor fermions ψ_a ($a = 1, \ldots, 4N$) in the LLL, possessing a maximal flavor symmetry of $\text{SU}(4N)$ alongside U(1) charge conservation. Next we introduce interactions that break the $\text{SU}(4N)$ symmetry down to $\text{Sp}(2N)$ symmetry. The $4N$-flavor fermions $\hat{\boldsymbol{\Psi}} = (\psi_1 \ldots \psi_{4N})^{\mathrm{T}}$ form an $\text{Sp}(2N)$ fundamental, resulting in $\hat{\boldsymbol{\Psi}}^{\mathrm{T}}\mathbf{J}\hat{\boldsymbol{\Psi}}$ being invariant under $\text{Sp}(2N)$ but not $\text{SU}(4N)$, where $\mathbf{J} = \begin{pmatrix} 0 & \mathbb{I}_{2N} \\ -\mathbb{I}_{2N} & 0 \end{pmatrix}$. Consequently, we can consider a Hamiltonian in the LLL with a

real space interaction,

$$H_{\text{int}} = \int d^2\vec{r}_1 \, d^2\vec{r}_2 \left[U(\vec{r}_{12})\hat{n}(\vec{r}_1)\hat{n}(\vec{r}_2) \right.$$
$$\left. - \frac{V(\vec{r}_{12})}{2N} \hat{\Delta}^\dagger(\vec{r}_1)\hat{\Delta}(\vec{r}_2) \right]. \quad (2)$$

where $\hat{n}(\vec{r}) = \hat{\boldsymbol{\Psi}}^\dagger(\vec{r})\hat{\boldsymbol{\Psi}}(\vec{r})$ and $\hat{\Delta}(\vec{r}) = \hat{\boldsymbol{\Psi}}^T(\vec{r})\mathbf{J}\hat{\boldsymbol{\Psi}}(\vec{r})$. For simplicity we consider the potentials to be both δ-functions $U(\vec{r}_{12}) = U\delta(\vec{r}_{12}), V(\vec{r}_{12}) = V\delta(\vec{r}_{12})$. The first term can be viewed as a continuum version of $SU(4N)$ Hubbard interaction on the lattice, which maintains the maximal $SU(4N)$ fermion flavor symmetry. The second term breaks $SU(4N)$ down to $Sp(2N)$ symmetry. It is worth noting that when $N = 1$ our model reduced to the $SO(5)$ NLσM studied in Ref. [30, 48], which is expressed in a slightly different form [50].

Let us now explain why Eq. (2) on LLL at half filling gives an $Sp(2N)$ Grassmannian NLσM with a level-1 WZW term. The $N = 1$ case has been discussed in Ref. [48, 51]. When $V = 0$, the dynamics of the system is captured by a NLσM on the $U(4N)$ Grassmannian $\frac{U(4N)}{U(2N)\times U(2N)}$,

$$S[\mathbf{Q}] = \frac{1}{g} \int d^2\vec{r} \, dt \, \text{Tr}(\partial^\mu \mathbf{Q}(\vec{r}, t))^2 + S_{\text{WZW}}[\mathbf{Q}]. \quad (3)$$

Here $\mathbf{Q}(\vec{r}, t)$ is a $4N \times 4N$ matrix field living on the $U(4N)$ Grassmannian, parameterized by

$$\mathbf{Q} = \mathbf{A}^\dagger \begin{pmatrix} \mathbb{I}_{2N} & 0 \\ 0 & -\mathbb{I}_{2N} \end{pmatrix} \mathbf{A}, \quad (4)$$

with A being a $U(4N)$ matrix. The matrix field $\mathbf{Q}(\vec{r}, t)$ encodes the occupation of fermions in our original system, specifically describing which $2N$ fermions out of the total $4N$ are occupied at the space-time coordinate $(\vec{r}, t)$. The same theory has also been proposed to describe the surface of certain $(3+1)$D symmetry protected topological phase [52]. The WZW term has a simple physical interpretation: the skyrmion, characterized by $\pi_2 \left(\frac{U(4N)}{U(2N)\times U(2N)} \right) = \mathbb{Z}$, is a fermion carrying a $U(1)$ electronic charge [53]. This generalizes a well-established result of the quantum Hall ferromagnet [54], which corresponds to the case of $N = 1/2$ in our scenario. Specifically, one can consider a special skyrmion that exhibits non-trivial patterns solely in the first two components of fermions, which then reduces to the familiar story of the quantum Hall ferromagnet.

Once a finite V is introduced, the global $SU(4N)$ symmetry is explicitly broken down to the $Sp(2N)$ symmetry. As a consequence, the matrix field $\mathbf{Q}(\vec{r}, t)$ becomes energetically favorable to fluctuate on the $Sp(2N)$ Grassmannian $\frac{Sp(2N)}{Sp(N)\times Sp(N)}$, which is a sub-manifold of the larger $U(4N)$ Grassmannian.

Additionally, the WZW term defined on the $U(4N)$ Grassmannian is also reduced to a WZW term on the $Sp(2N)$ Grassmannian. Therefore, even at finite V, the system can still be effectively described by Eq. (3), where the matrix field $\mathbf{Q}(\vec{r}, t)$ resides on the $Sp(2N)$ Grassmannian and is parameterized by

$$\mathbf{Q} = \mathbf{M}^T \begin{pmatrix} \mathbf{J}_N & 0 \\ 0 & -\mathbf{J}_N \end{pmatrix} \mathbf{M}, \quad \mathbf{M} \in Sp(2N). \quad (5)$$

The parameter g characterizes the stiffness of the NLσM and, phenomenologically, it is controlled by V/U in our original model given by Eq. (2). The specific value of g will determine the phase of the system, which we will discuss in further detail later.

Having understood how to realize the $Sp(2N)$ Grassmannian NLσM on the LLL, we are now ready to extend it to the sphere. In practice, we simply consider the LLL on a sphere with a $4\pi s$ monopole placed at the center [55] (Fig. 1a). The LLL on the sphere consists of $N_{\text{orb}} = 2s + 1$ degenerate orbitals, which can be described by the monopole harmonics $Y_{sm}^{(s)}(\theta, \varphi)$ [56], where $m = -s, -s + 1, \cdots, s$. These $2s + 1$ orbitals form a spin-s irreducible representation of the $SO(3)$ sphere rotation. On the sphere, we can parameterize the system using spherical coordinates (θ, φ), and we have $d^2\vec{r} = N_{\text{orb}} \sin\theta \, d\theta \, d\varphi$, and $\delta(\vec{r}_{12}) = \frac{1}{N_{\text{orb}}}\delta(\cos\theta_1 - \cos\theta_2)\delta(\varphi_1 - \varphi_2)$. Here, we utilize the fact that on the spherical LLL, the sphere radius R and the Landau orbital number N_{orb} are physically equivalent, i.e., $N_{\text{orb}} \sim R^2$.

Next we project the interaction Eq. (2) onto the LLL on sphere,

$$\hat{\boldsymbol{\Psi}}(\theta, \varphi) = \frac{1}{\sqrt{N_{\text{orb}}}} \sum_{m=-s}^{s} \bar{Y}_{sm}^{(s)}(\theta, \varphi)\hat{\mathbf{c}}_m. \quad (6)$$

Here $\hat{\mathbf{c}}_m = (c_{m,1}, \cdots, c_{m,4N})$ is the second quantized fermion operator defined on the Landau orbitals. The normalization factor $1/\sqrt{N_{\text{orb}}}$ is to ensure the particle density $\hat{n}(\vec{r}) = \hat{\boldsymbol{\Psi}}^\dagger(\vec{r})\hat{\boldsymbol{\Psi}}(\vec{r})$ is an intensive quantity. Rewriting the interaction Hamiltonian in a second quantized form in terms of $\hat{\mathbf{c}}_m$, we get
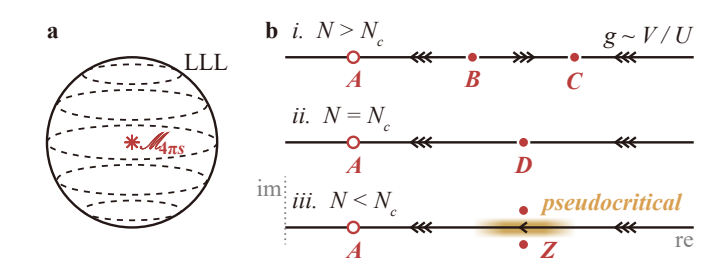

FIG. 1. (a) An illustration of the fuzzy sphere setup. (b) Possible scenarios of the RG flow of the $Sp(N)$ model as a function of V/U: (i) At $N > N_c$, there is a symmetry-breaking fixed point A, a repulsive B and an attractive C CFT fixed points; (ii) at $N = N_c$, the CFT fixed points B and C merges into a single fixed point D; (iii) at $N < N_c$, D splits into two complex fixed points Z, and the region in vicinity exhibits pseudo-critical behavior. Here the filled and empty circles denote CFT and non-CFT fixed points.

$$H_{\text{int}}^{(\text{LLL})} = \sum_{m_1 m_2 m_3 m_4} \left(U_{m_1 m_2 m_3 m_4} (\hat{\mathbf{c}}_{m_1}^\dagger \hat{\mathbf{c}}_{m_4})(\hat{\mathbf{c}}_{m_2}^\dagger \hat{\mathbf{c}}_{m_3}) - V_{m_1 m_2 m_3 m_4} (\hat{\mathbf{c}}_{m_1}^\dagger \mathbf{J}^\dagger \hat{\mathbf{c}}_{m_2}^\dagger)(\hat{\mathbf{c}}_{m_3} \mathbf{J} \hat{\mathbf{c}}_{m_4}) \right). \tag{7}$$

The parameter $U_{m_1 m_2 m_3 m_4}$ is connected to the Haldane pseudopotential U_l by

$$U_{m_1 m_2 m_3 m_4} = \sum_l U_l (4s - 2l + 1) \begin{pmatrix} s & s & 2s - l \\ m_1 & m_2 & -m_1 - m_2 \end{pmatrix} \begin{pmatrix} s & s & 2s - l \\ m_4 & m_3 & -m_4 - m_3 \end{pmatrix}, \tag{8}$$

where $\begin{pmatrix} j_1 & j_2 & j_3 \\ m_1 & m_2 & m_3 \end{pmatrix}$ is the Wigner $3j$ symbol, and similarly $V_{m_1 m_2 m_3 m_4}$ is connected to the Haldane pseudopotential V_l. For the case of δ potential we choose, the only non-zero component of the Haldane pseudopotential is $l = 0$.

At last, let us comment on why the LLL projection (truncation) leads to a fuzzy sphere. It is instructive to consider the projection of the coordinates of a unit sphere, denoted as $\vec{x} = (\sin\theta\cos\varphi, \sin\theta\sin\varphi, \cos\theta)$. After the projection, the coordinates are transformed into $(2s + 1) \times (2s + 1)$ matrices, where $(\vec{X})_{m_1, m_2} = \int \sin\theta \, d\theta \, d\varphi \, \vec{x} \, \bar{Y}_{s,m_1}^{(s)}(\theta, \varphi) Y_{s,m_2}^{(s)}(\theta, \varphi)$. These matrices satisfy the following relations:

$$[\mathbf{X}^\mu, \mathbf{X}^\nu] = \frac{1}{s+1} i\epsilon^{\mu\nu\rho} \mathbf{X}_\rho, \quad \mathbf{X}_\mu \mathbf{X}^\mu = \frac{s}{s+1} \mathbf{1}_{2s+1}. \tag{9}$$

The fact that the three coordinates satisfy the SO(3) algebra formally defines a fuzzy sphere [43]. It is worth noting that in the thermodynamic limit $s \to \infty$, the fuzziness disappears and a unit sphere is recovered.

B. Conformal window and pseudo-criticality

As conjectured in Ref. [57], the generic phase diagram of a 3D NLσM with a WZW term can be summarized in Fig. 1b, which contains three different situations, depending on the value of N:

i. $N > N_c$. For N larger than a critical value N_c, there exist three different fixed points as we tune the NLσM coupling g, or equivalently V/U in our model. When g is small, the NLσM spontaneously breaks the global symmetry, and the ground state manifold corresponds to the target space of the NLσM (in our case, the Sp($2N$) Grassmannian). This corresponds to the attractive fixed point A. On the other hand, when g is large, the system flows to the attractive fixed point C, which is fully symmetric and described by a 3D CFT. For the Sp($2N$) Grassmannian NLσM considered in our paper, this attractive conformal fixed point is in the same universality class as a QCD$_3$ theory with $2N$ flavors of Dirac fermions coupled to an SU(2) gauge field [53, 57]. In the limit of $N \gg 1$, the operator spectrum can be computed using the standard large-N expansion technique [58]. At a critical coupling g_c, there is a repulsive fixed point B, which also corresponds to a fully symmetric CFT. This fixed point describes the phase transition between the CFT phase (C) and the spontaneous symmetry-breaking phase (A).

ii. $N = N_c$. When decreasing N to a critical value $N = N_c$, the two CFT fixed points B and C merge into one (D) and the singlet S become exactly marginal ($\Delta_S = 3$).

iii. $N < N_c$. For $N < N_c$, the fixed point D splits into two fixed points located in the complex plane, denoted Z. Along the real axis, there are no CFT fixed points. However, the complex fixed points Z are described by complex CFTs, which have complex conformal data including complex scaling dimensions [34, 35]. When Z is sufficiently close to the real axis, these complex conformal data have a very small imaginary part. Importantly, the RG flow near Z is slow, and over a large length scale, the system exhibits an approximate conformal symmetry with conformal data that closely resembles the real part of the complex CFT's complex conformal data. This behavior, referred to as pseudo-criticality or "walking behavior", is conjectured to account for the anomalous scaling observed numerically in the DQCP. A similar phenomenon has been observed in the 2D 5-state Potts model [37].

So the key question pertains to the value of N_c for the Sp($2N$) Grassmannian NLσM. If $N_c < 1$, the SO(5) DQCP corresponds to a genuine continuous transition described by the attractive conformal fixed point C shown in Fig.1b, i. On the other hand, if $N_c > 1$, the SO(5) DQCP exhibits pseudo-critical behavior as depicted in Fig.1b, iii. We also note that such N-dependent phase diagrams are believed to be common in various models and theories. For instance, in critical gauge theories involving Dirac fermions (or critical bosons) coupled to a dynamical gauge field $G(k) = $ SU(k), U(k), Sp(k), etc., there exists a critical value $N_c(G(k))$ for each gauge group [59]. Our Sp($2N$) Grassmannian NLσM corresponds to $2N$ Dirac fermions coupled to an SU(2) gauge field. However, determining the precise region of the conformal window $(N > N_c(G(k)))$ for any gauge theory has been a longstanding challenge in the field. The main difficulty lies in distinguishing between pseudo-critical behavior and true critical behavior: the former also exhibits an approximate conformal symmetry over a large length scale, while the conformal symmetry of the latter is exact only in the thermodynamic limit.

Here, we propose that the fuzzy sphere microscope can be used to resolve the outstanding puzzle of the conformal window. The idea is to examine the RG flow as well as the scaling dimension Δ_S of the lowest-lying singlet S of the global symmetry. The smoking gun evidence for pseudo-criticality is that, at the coupling V/U on the right-hand side of the vicinity of the complex fixed points Z, Δ_S will flow from being slightly irrelevant (i.e., $\Delta_S \gtrsim 3$) to slightly relevant (i.e., $\Delta_S \lesssim 3$) as the system size increases [60]. Such flow will not occur in the case of $N > N_c$, as one will have either $\Delta_S > 3$ or Δ_S flowing from being relevant to irrelevant as the system size increases. The latter situation corresponds to the coupling being close

to the critical coupling of the repulsive fixed point B. In this paper, we will focus on the case $N = 1$, where we find a clear signature of pseudo-criticality.

C. Relation to the original story of DQCP

DQCP was originally proposed to describe a direct continuous transition between a Néel phase and VBS phase on the square lattice [2, 3]. The effective field theory is the CP^1 model, which is a gauge theory that has $N_f = 2$ flavors of complex critical bosons coupled to a U(1) gauge field. This field theory has an explicit SU(2) × U(1) global symmetry, where SU(2) is the flavor rotation symmetry between the two flavors of bosons, and U(1) is also called the topological U(1) corresponding to the flux conservation of the U(1) gauge field. For the Neel-VBS transition on the square lattice, there is only an SU(2) × $\mathbb{Z}_4$ symmetry in the UV, where SU(2) is the spin-rotation symmetry, while $\mathbb{Z}_4$ is the square lattice C_4 rotation symmetry. At the phase transition, it is conjectured that $\mathbb{Z}_4$ is enhanced to U(1), which means that the 8π-monopole $\mathscr{M}_{8\pi}$ has to be irrelevant. Similarly, for the Neel-VBS transition on the honeycomb lattice [21, 26], where there is only a C_3 lattice rotation, the 6π-monopole $\mathscr{M}_{6\pi}$ has to be irrelevant if it is described by the DQCP.

More recently, it was numerically discovered that the SU(2) × U(1) symmetry enhances to the SO(5) symmetry [7], and it inspired a number of new dual descriptions of DQCP [8], including the SO(5) NLσM studied here. In the original Neel-VBS transition, the SO(5) symmetry corresponds to the symmetry between the 3-component Neel order parameter and the 2-component VBS order parameter. The WZW term encodes the physics of intertwinement between the Neel and VBS orders, namely, the topological defect of one binds the symmetry charge of the other [61–63]. One component of the SO(5) rank-2 symmetric traceless tensor becomes SU(2) × U(1) singlet, so it is the tuning operator for the Neel-VBS transition. In our model, this operator is not allowed by the SO(5) symmetry, so there is no relevant singlet if the DQCP is a genuine critical point without further fine-tuning.

It is also worth noting that the DQCP exhibits a mixed anomaly between the SO(5) and time-reversal symmetry [8]. In the Neel-VBS transition, apart from time-reversal symmetry, there is only an SU(2) × $\mathbb{Z}_4$ symmetry in the UV, which is consistent with this anomaly. Interestingly, the SO(5) NLσM possesses exact SO(5) and time-reversal symmetry (i.e., particle-hole symmetry) in the UV, which appears to contradict the anomaly of DQCP. The way to reconcile this contradiction is by understanding that the particle-hole symmetry on the LLL is a non-local symmetry [64]. Similar physics also applies to the Sp(2N) Grassmannian NLσM, which realizes $2N$ flavor SU(2) QCD_3 with exact Sp(2N) and time-reversal symmetry in the UV. In contrast, for a lattice realization of QCD_3, one can only have Sp(N) × Sp(N) symmetry in the UV due to the parity anomaly.

III. NUMERICAL RESULTS

A. Exact diagonalization and quantum numbers

We perform an exact diagonalization calculation for the Hamiltonian Eq. (2) at $N = 1$ to get the lower spectra up to a system size $N_{\text{orb}} = 9$ and look at the 3600 lowest lying states for $N_{\text{orb}} \leq 8$ and the 180 lowest lying states for $N_{\text{orb}} = 9$. As each eigenstate carries a definite quantum number of all the symmetries of the Hamiltonian, and implementing the corresponding conversed quantities can divide the Hilbert space into sectors and block-diagonalize the Hamiltonian, it is useful to first analyze the symmetries of the Hamiltonian:

(1) The SO(3) rotation symmetry of S^2. The angular momentum of the state can be determined by measuring the SO(3) quadratic Casimir $\langle \Phi | \hat{L}^2 | \Phi \rangle = \ell_\Phi(\ell_\Phi + 1)$. In the calculation, we implement the conservation of $\hat{L}^z$ which gives each state a quantum number $m_\Phi^z = \langle \Phi | \hat{L}^z | \Phi \rangle$ (cf. Appendix A).

(2) The SO(5) = Sp(2)/$\mathbb{Z}_2$ flavor symmetry. The SO(5) representation carried by the operator (state) is determined by the counting degeneracy of the corresponding states and by measuring the SO(5) quadratic Casimir. In this paper, we label the representations by their dimensions, namely, the singlet representation **1**, the SO(5) vector representation (i.e., the Sp(2) antisymmetric rank-2 traceless tensor representation) **5**, the SO(5) antisymmetric rank-2 tensor representation (i.e., the Sp(2) symmetric rank-2 tensor representation) **10**, the SO(5) symmetric rank-2 traceless tensor representation **14**. In the calculation, we implement two commuting conserved quantities $\sigma^{1,2}$ (cf. Appendix A) due to this symmetry, corresponding to the two generators of the Cartan subalgebra of $\mathfrak{so}(5)$.

(3) The particle-hole symmetry $\mathscr{P} : \hat{\mathbf{c}}_m \to \mathbf{J}\hat{\mathbf{c}}_m^*, i \to -i$.

With these conserved quantities L^z and $\sigma^{1,2}$ implemented, the $N_{\text{orb}} = 9$ calculation takes 168 GB of memory and 843 seconds (using 2.4Hz Intel(R) Xeon(R) Gold 6148 CPU with 40 cores) to produce the 10 lowest eigenstates in the maximal sector $(m^z, \sigma^1, \sigma^2) = (0, 0, 0)$.

B. Phase diagram

To study the physics of DQCP, we should first identify a region in the phase diagram that does not show spontaneous symmetry breaking. So we look at the SO(5) symmetry-breaking order parameter (i.e. SO(5) vector),

$$m^i = \sum_m \hat{\mathbf{c}}_m^\dagger \gamma^i \hat{\mathbf{c}}_m, \tag{10}$$

where the γ-matrices are $\{\mathbb{I} \otimes \tau^x, \mathbb{I} \otimes \tau^z, \sigma^x \otimes \tau^y, \sigma^y \otimes \tau^y, \sigma^z \otimes \tau^y\}$. In a quantum system described by a unitary CFT, the order parameter should scale with the linear scale of the system as $\langle m^2 \rangle \sim R^{2\Delta_\phi} = N_{\text{orb}}^{\Delta_\phi}$, where ϕ is the lowest parity-odd scalar SO(5) vector operator in the CFT. We can similarly look at the one-point function $\langle \phi | m | 0 \rangle \sim R^{-\Delta}$, where $|\phi\rangle$ is the state corresponding to the ϕ operator in the CFT. As its scaling dimension is bounded by the unitarity bound $\Delta_\phi \geq d/2 - 1 = 1/2$ [32], $\langle m^2 \rangle N_{\text{orb}}^{1/2}$ and $\langle \phi | m | 0 \rangle N_{\text{orb}}^{1/4}$ should be
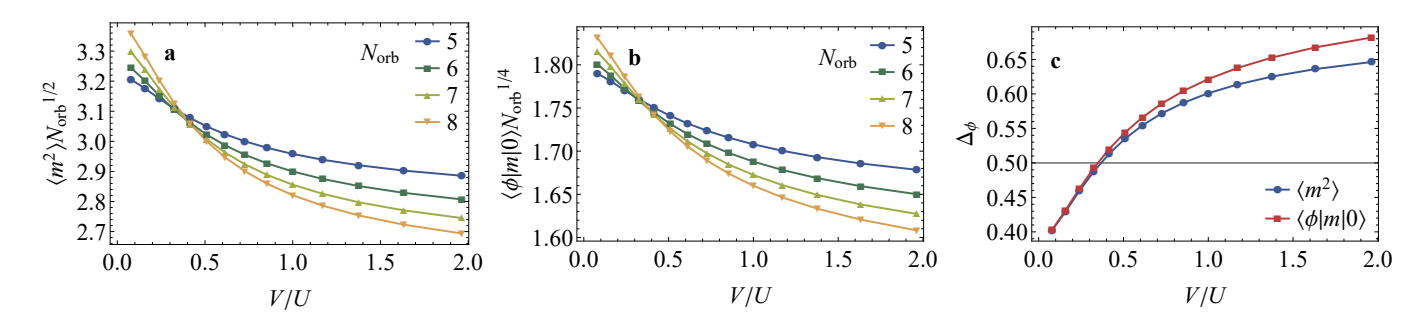
FIG. 2. Identifying a disorder region by finite-size scaling of the order parameter SO(5) vector m. (a) $\langle m^2 \rangle N_{\text{orb}}^{1/2}$ and (b) $\langle \phi | m | 0 \rangle N_{\text{orb}}^{1/4}$ as a function of V/U at $N_{\text{orb}} = 5, 6, 7, 8$. (c) The scaling dimension Δ_ϕ as a function of V/U extracted from the finite-size scaling of $\langle m^2 \rangle$ and $\langle \phi | m | 0 \rangle$.
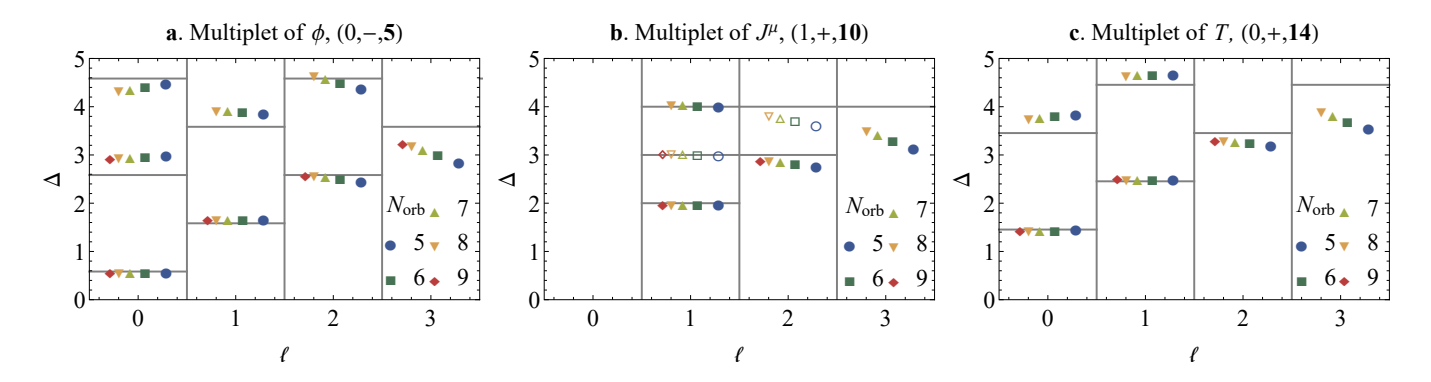

FIG. 3. The scaling dimensions of the conformal multiplet of (a) the lowest SO(5) vector ϕ, (b) the SO(5) symmetry current J and (c) stress tensor T at different spin ℓ and system size N_{orb}. Certain high-lying states of the largest size $N_{\text{orb}} = 9$ are beyond our computation capacity. The horizontal grey bar denotes the anticipated values based on the integer-spaced levels from the conformal symmetry. The filled and empty symbols in (b) signify the parity-even and parity-odd descendants. Parameter V/U is taken such that $\Delta_{\mathcal{T}} = 3$ exactly.

decreasing with N_{orb}. Numerically, we observe these two quantities increase with N_{orb} at $V/U \lesssim 0.4$, corresponding to a symmetry-breaking region, and decrease with N_{orb} at $V/U \gtrsim 0.5$ (Fig. 2a,b). We also perform a finite-size scaling to fit the scaling dimension Δ_ϕ (Fig. 2c). These results consistently indicate that SO(5) symmetry is not breaking at $V/U > 0.5$. Consequently, we will focus on this region in the following.

C. Approximate conformal symmetry

To verify whether or not the $V/U \gtrsim 0.5$ region is described by a CFT, we need to examine if the energy spectrum has an emergent conformal symmetry, namely if they form irreducible representations of the conformal group. We first determine the size and parameter-dependent factor in Eq. (1) by setting the scaling dimension of the SO(5) symmetry current to be exactly $\Delta_J = 2$. The symmetries of the Hamiltonian should be identified with the symmetries of the conformal field theory, and so are the quantum numbers carried by the quantum states and by the CFT operators. In particular, the SO(3) rotation symmetry of S^2 is identified with the Lorentz rotation of the conformal group, and the angular momentum is identified with the Lorentz spin ℓ; the particle-hole symmetry acts as an improper $\mathbb{Z}_2$ of O(3) and is thus identified as the spacetime parity

$\mathscr{P}$ of the CFT [42].

One convincing evidence for the conformal symmetry is the integer-spaced levels (e.g., see Ref. [42] for a detailed discussion). In a CFT spectrum, for any scalar primary Φ with quantum numbers $(\ell = 0, \mathscr{P}, \text{rep.}; \Delta)$, its descendants can be written in the form of $\partial^{\nu_1} \ldots \partial^{\nu_j} (\partial^2)^n \Phi$ $(n, j \geq 0)$ with quantum numbers $(j, \mathscr{P}, \text{rep.}; \Delta + 2n + j)$; for spinning primary $\Phi^{\mu_1 \cdots \mu_\ell}$, its descendants can be written either as $\partial^{\nu_1} \ldots \partial^{\nu_j} (\partial^2)^n \partial_{\mu_1} \ldots \partial_{\mu_i} \Phi^{\mu_1 \cdots \mu_\ell}$ $(0 \leq i \leq \ell, n, j \geq 0)$ with quantum numbers $(\ell - i + j, \mathscr{P}, \text{rep.}; \Delta + 2n + i + j)$ or as $\epsilon_{\mu_1 \rho \sigma} \partial^\rho \partial^{\nu_1} \ldots \partial^{\nu_j} (\partial^2)^n \partial_{\mu_2} \ldots \partial_{\mu_i} \Phi^{\mu_1 \cdots \mu_\ell}$ $(1 \leq i \leq \ell, n, j \geq 0)$ with quantum numbers $(\ell - i + j + 1, -\mathscr{P}, \text{rep.}; \Delta + 2n + i + j)$; for conserved currents like SO(5) symmetry current J^μ and stress tensor $\mathscr{T}^{\mu\nu}$, only $i = 0$ descendants exist due to the conservation $\partial_{\mu_1} \Phi^{\mu_1 \cdots \mu_\ell} = 0$.

Numerically, we observe that the low-lying levels indeed exhibit a remarkable alignment with the integer-spaced patterns predicted by the conformal symmetry. Fig. 3 shows numerically identified conformal multiplet (i.e. primary and its descendants) of the lowest SO(5) vector ϕ, the lowest SO(5) traceless tensor T and the symmetry current J^μ by matching the quantum numbers. For each system size N_{orb}, the data is measured at a size-dependent parameter value V/U around 0.9 such that $\Delta_{\mathscr{T}} = 3$ holds exactly, which is another requirement of conformal symmetry. We are able to find all their

descendants up to $\ell \leq 3$ and $\Delta \leq 5$ with none missing. The measured scaling dimensions (symbols) and the corresponding anticipated values (grey lines) exhibit good agreement. More conformal multiplets like these are summarized in Table VI in the appendix, which contains 19 primaries and 82 conformal descendants. These results convincingly demonstrate the emergent conformal symmetry.

We remark that certain intervals do not have the expected trend when increasing the system size (e.g., $\Delta_{\partial^\mu \phi} - \Delta_\phi$ scales to approximately 1.1). This may come from either insufficiently large system size or the lack of exact conformal symmetry due to the pseudo-criticality (see discussion below). It is also worth noting that if we move away from this parameter point, approximate conformal symmetry still holds in a vast region. We examine scaling dimension of the stress tensor $\mathscr{T}^{\mu\nu}$ and two descendants $\partial^\mu \phi$ and $\epsilon^{\mu\nu\rho} \partial_\nu J_\rho$ and compare them with the anticipated values (Fig. 4a,c,d). For $\mathscr{T}^{\mu\nu}$, the agreement holds with a maximal discrepancy of 5% for a vast region $0.7 < V/U < 1.5$, and the error decreases with increasing $N_{\rm orb}$; for $\epsilon^{\mu\nu\rho} \partial_\nu J_\rho$, the agreement holds with a maximal discrepancy of 3%.

Our observation provides strong support for an approximate conformal symmetry in a vast region $0.7 < V/U < 1.5$. The next question we want to answer is whether this CFT signa-
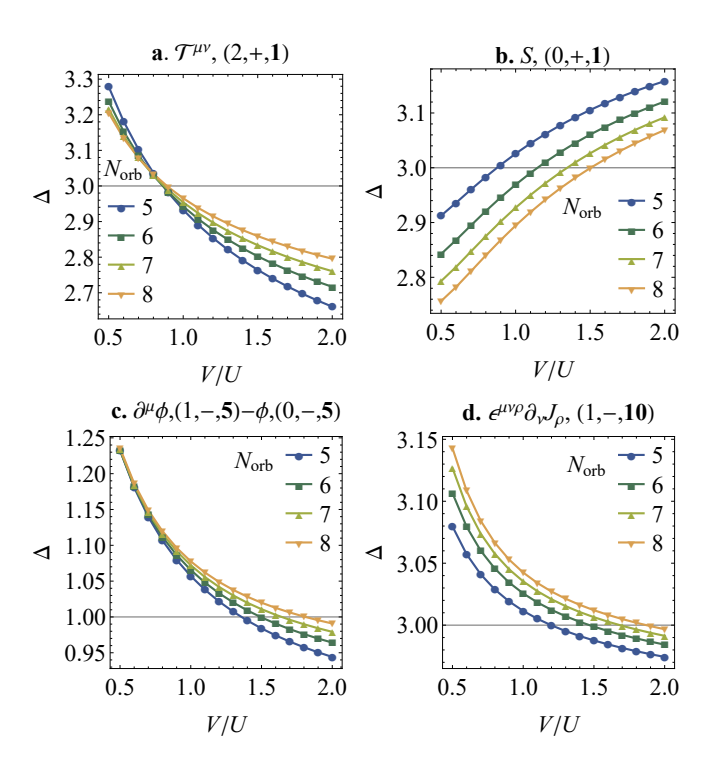
TABLE I. The scaling dimensions Δ_S of the lowest singlet S at different V/U and system size $N_{\rm orb}$ calibrated by the scaling dimension of the symmetry current $\Delta_J = 2$. The empty entry is beyond our calculation capacity.

V/U	$N_{\rm orb}$				
	9	8	7	6	5
0.700	2.782	2.811	2.847	2.895	2.960
0.915	2.845	2.872	2.906	2.949	3.009
1.011	2.871	2.897	2.930	2.972	3.028
1.500	2.977	2.999	3.026	3.061	3.106
3.000	3.136	3.151	3.170	3.193	3.221
10.00		3.286	3.297	3.308	3.321

ture corresponds to the fixed point B (a phase transition), C (a genuine SO(5) CFT) or Z (pseudo-criticality) in Fig. 1b. The vast region of approximate conformal symmetry rules out the possibility of an unstable fixed point B that needs fine tuning. The distinction between a genuine SO(5) CFT and pseudo-criticality can be further diagnosed by the lowest singlet S. In the former case, Δ_S will increase towards irrelevance, with $\Delta_S > 3$, while in the latter case, Δ_S will decrease towards relevance, with $\Delta_S < 3$. Our results show that as $N_{\rm orb}$ increases or V/U decreases, its scaling dimension decrease towards relevant $\Delta_S \lesssim 3$ (Fig. 4b and Table II). In particular, for $1.0 \lesssim V/U \lesssim 1.5$, it flows from slightly irrelevant ($\Delta_S \gtrsim 3$) to slightly relevant ($\Delta_S \lesssim 3$) as the system size increases, which is a smoking gun evidence for the pseudo-criticality. Hence, our numerical result is more consistent with the scenario that DQCP corresponds to not a real CFT, but to a pseudo-critical region that locates near complex CFT fixed points and exhibits approximate conformal symmetry. However, we cannot completely rule out the scenario in which $N \gtrsim N_c$, resulting in the two conformal fixed points B and C being very close to each other. This is because Δ_S could exhibit a slightly non-monotonic behavior that was not captured due to the limitations of the system size, although we have not found any indication of it.

D. Operator spectrum

Having presented the evidence that DQCP is likely pseudo-critical, we now turn to its (pseudo-)critical properties, i.e., scaling dimensions of primary operators. Since there are no true CFT fixed points in the real axis, the operator spectrum presented below should be viewed as the real part of the complex scaling dimensions of the true complex CFTs. We also note that the scaling dimensions of the operators change with the parameter V/U (Fig. 5), this may be the result of the walking behavior in the vicinity of the complex fixed point. The parameter dependence of scaling dimensions of various primaries appears to follow the same pattern, suggesting a potential universal behavior that can be understood through RG analysis.

As we target the pseudo-critical region in the RG flow dia-

FIG. 4. The scaling dimension of (a) stress tensor $\mathscr{T}^{\mu\nu}$, (b) the lowest scalar S, (c) the diffence between the lowest SO(5) vector ϕ and its descendant $\partial^\mu \phi$ and (d) the descendant $\epsilon^{\mu\nu\rho} \partial_\nu J_\rho$ of the symmetry current as a function of V/U at different system size $N_{\rm orb}$ calibrated by the scaling dimension of the symmetry current $\Delta_J = 2$. The quantum numbers $(\ell, \mathscr{P}, \text{rep.})$ are given in the bracket. The grey gridline in (a), (c) and (d) indicates the values imposed by the conformal symmetry, and the grey gridline in (b) indicates $\Delta = 3$ that separates relevance and irrelevance.

gram, to minimize the finite-size effect, for each system size N_{orb}, we conduct the calculation at a V/U value where $\Delta_{\mathscr{T}} = 3$ holds exactly. We analyze the operators through the following process: (1) We pick out the lowest state in each representation and identify it as a primary; (2) we identify its descendants by matching the quantum numbers $(\ell, \mathscr{P}, \text{rep.}; \Delta)$; (3) we remove the identified conformal multiplet from the spectrum and repeat the process. The lowest-lying primaries are listed in Table II. We complement this table with two other operators $\mathscr{M}_{8\pi}$ and S^- which will be explained in the following. The full spectrum can be found in Appendix B.

Besides J^μ, $\mathscr{T}^{\mu\nu}$ and S that we have introduced before, there are several other primary operators worth noting:

(1) The lowest $\ell = 0$ parity-odd SO(5) vector ϕ corresponds to the order parameter. Its scaling dimension is related to the anomalous dimension $\eta = (\Delta_\phi - 1/2)/2$. Our $N_{\text{orb}} = 9$ data implies $\eta = 0.168$.

(2) The lowest $\ell = 0$ parity-even symmetric rank-2 tensor T corresponds to the relevant perturbation that controls the original Neel-VBS transition. Its scaling dimension is related to the exponent $\nu = 1/(3 - \Delta_T)$. Our $N_{\text{orb}} = 9$ data implies $\nu = 0.647$.

(3) The lowest $\ell = 0$ parity-odd operator in ⬚⬚⬚ representation corresponds to the 6π-monopole $\mathscr{M}_{6\pi}$ in the CP^1 description. This operator is forbidden in lattices with C_4 rotation symmetry but allowed for C_3 symmetry. Although the exact value of its scaling dimension flows (Fig. 5c), our calculation
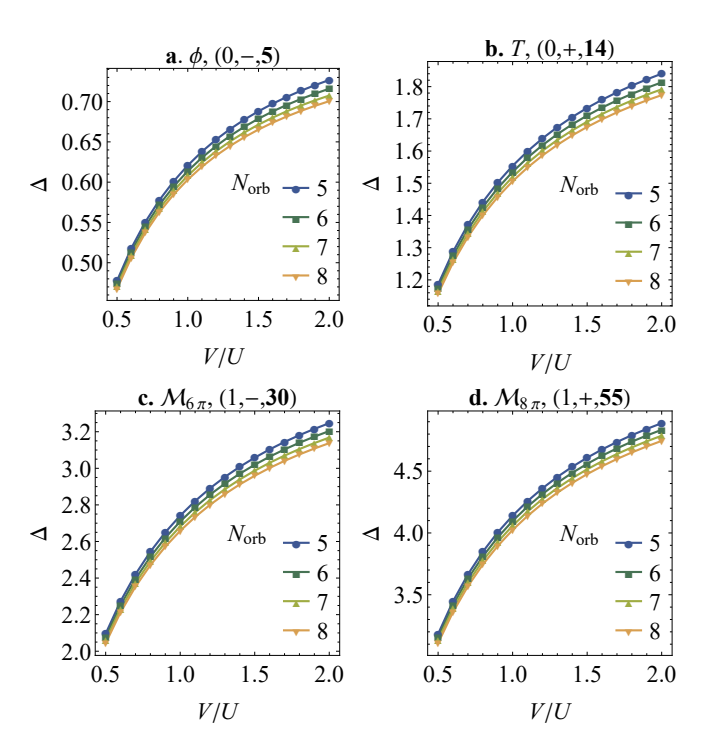
TABLE II. The scaling dimension and quantum numbers for the lowest lying primary operators obtained from state-operator correspondence at different system size N_{orb}. These numbers still violate bootstrap bound. Parameter V/U is taken such that $\Delta_{\mathscr{T}} = 3$ exactly. The empty entry is beyond our calculation capacity.

			N_{orb}	9	8	7	6	5
			V/U	0.9150	0.8904	0.8717	0.8617	0.8644
Op.	ℓ	$\mathscr{P}$	Rep.			Δ		
$\mathbb{I}$	0	+	**1**	0.000	0.000	0.000	0.000	0.000
ϕ	0	−	**5**	0.584	0.583	0.583	0.586	0.593
T	0	+	**14**	1.454	1.452	1.455	1.463	1.482
J^μ	1	+	**10**	2.000	2.000	2.000	2.000	2.000
$\mathscr{M}_{6\pi}$	0	−	**30**	2.565	2.562	2.567	2.582	2.614
S	0	+	**1**	2.845	2.865	2.894	2.937	2.998
$\mathscr{T}^{\mu\nu}$	2	+	**1**	3.000	3.000	3.000	3.000	3.000
	1	−	**35**	3.028	3.028	3.030	3.037	3.051
	1	+	**10**	3.167	3.171	3.176	3.183	3.192
	2	+	**14**	3.330	3.325	3.315	3.283	3.216
$\mathscr{M}_{8\pi}$	0	+	**55**	3.885	3.881	3.887	3.908	3.952
S^-	0	−	**1**		5.366	5.373	5.372	5.352

finds it relevant in all cases, which is likely to imply that the DQCP is not possible on honeycomb lattice as $\mathscr{M}_{6\pi}$ will drive it away [21, 26].

(4) The lowest $\ell = 0$ parity-even operator in ⬚⬚⬚⬚ representation corresponds to the 8π-monopole $\mathscr{M}_{8\pi}$ in the CP^1 description. This operator is related to the dangerous irrelevant perturbation in the Néel-VBS DQCP [2, 3]. Although the exact value of its scaling dimension flows (Fig. 5d), our calculation confirms its irrelevance.

(5) The lowest $\ell = 0$ parity-odd singlet S^- corresponds to the fermion bilinear in the QCD_3 description. This operator has engineering dimension 2, but receives a huge correction up to $\Delta_{S^-} \approx 5.37$ [65]. If this operator were relevant, it would drive the DQCP towards a chiral spin liquid, potentially playing a role in interesting phenomena observed in real materials [49]. Our calculation finds it highly irrelevant and therefore negates this scenario.

It is worth noting that the scaling dimensions of various monopoles in the CP^1 description have been calculated by introducing such defects into 3D critical dimer model in Monte Carlo simulation [23, 24], including $\Delta_\phi = 0.579(8)$, $\Delta_T = 1.52(7)$ and $\Delta_{\mathscr{M}_{6\pi}} = 2.80(3)$, which are very close to our results and also confirm the relevance of 6π-monopole. We can also compare the critical exponents with the Monte Carlo results in various transitions, including 3D loop model $\eta_{\text{loop, VBS}} = 0.25(3)$, $\eta_{\text{loop, Néel}} = 0.259(3)$, $\nu_{\text{loop, VBS}} = 0.503(9)$ and $\nu_{\text{loop, Néel}} = 0.477(4)$ [22], J-Q model $\eta_{J\text{-}Q} = 0.35$, $\nu_{J\text{-}Q} = 0.455(2)$ [14, 25, 66] and transition between quantum spin Hall insulators and s-wave superconductor (QSH-SC) [67] $\nu_{\text{SC}} = 0.56(6)$, $\nu_{\text{QSH}} = 0.6(1)$, $\eta_{\text{SC}} = 0.22(6)$ and $\eta_{\text{QSH}} = 0.21(5)$ [28]. We think that the discrepancy between these results is a consequence of pseudo-criticality. Specifically, we find scaling dimensions drifting

FIG. 5. The scaling dimension of (a) the lowest SO(5) vector ϕ, (b) the lowest rank-2 SO(5) symmetric traceless tensor T, (c) the 6π-monopole $\mathscr{M}_{6\pi}$ and (d) the 8π-monopole $\mathscr{M}_{8\pi}$ as a function of V/U at different system size N_{orb} calibrated by the scaling dimension of the symmetry current $\Delta_J = 2$. The quantum numbers $(\ell, \mathscr{P}, \text{rep.})$ are given in the bracket.
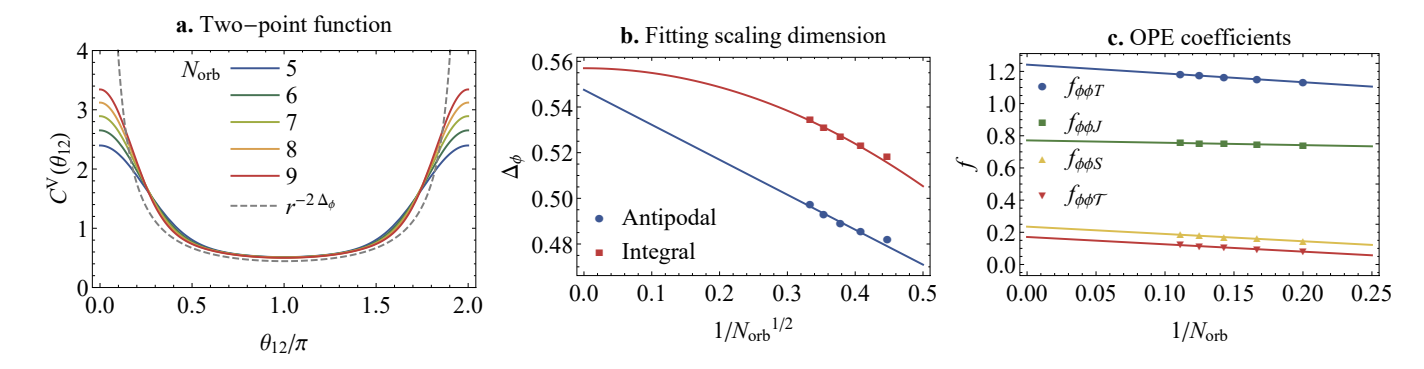
FIG. 6. (a) The dimensionless two-point correlation function $C^V(\theta_{12})$ defined in Eq. (15) at different system size N_{orb} and the theoretical expectation in the thermodynamic limit $C(\theta_{12}) = (2\sin\frac{\theta_{12}}{2})^{-2\Delta_\phi}$; (b) the scaling dimension Δ_ϕ extrapolated from its value at antipodal points Eq. (16) and spatial integral Eq. (17); (c) The finite-size scaling of OPE coefficients $f_{\phi\phi T}$, $f_{\phi\phi J}$, $f_{\phi\phi S}$ and $f_{\phi\phi \mathcal{T}}$.

with UV interacting V/U and system size. Similar drift with system size has also been observed in ν in loop models [22] and both η and ν in the QSH-SC transition [28]. As evidence, the anomalous dimension η measured at $V/U \approx 1.2$ is close to the loop model results and $V/U \approx 1$ is close to the QSH-SC transition results. It will be interesting to extract more stable scaling dimensions by studying the complex fixed point directly or by extrapolating data based on the RG analysis.

E. Correlation functions and OPE coefficients

Having studied the spectrum of the system and the corresponding CFT, we now turn to the operators and their correlation functions. The simplest particle-hole symmetric operator is the density operator [46]

$$\hat{n}^M(\theta, \varphi) = \hat{\Psi}^\dagger(\theta, \varphi)M\hat{\Psi}(\theta, \varphi), \qquad (11)$$

where M is an Hermitian matrix insertion. Any gapless density operator in the microscopic model can be expressed as a linear combination of CFT operators including primaries and descendants that have the same parity and SO(5) quantum number as $\hat{n}^M$

$$\hat{n}^M(\theta, \varphi; \tau = 0) = \sum_\alpha c_\alpha \hat{\Phi}_\alpha. \qquad (12)$$

Using this decomposition, we may consider the one-point functions

$$\langle \Phi_\alpha | \hat{n}^M(\theta, \varphi; \tau = 0) | 0 \rangle = \sum_{\beta \in [\alpha]} c_\beta R^{-\Delta_\beta} h_\beta(\theta, \varphi),$$

$$\langle \Phi_\alpha | \hat{n}^M(\theta, \varphi; \tau = 0) | \Phi_\gamma \rangle = \sum_\beta f_{\alpha\beta\gamma} c_\beta R^{-\Delta_\beta} \tilde{h}_{\alpha\beta\gamma}(\theta, \varphi),$$

$$(13)$$

where $|\Phi_\alpha\rangle$ denotes the state corresponding to the CFT operator $\hat{\Phi}_\alpha$, $[\alpha]$ denotes conformal multiplet of α, $h_\beta(\theta, \varphi)$ and $\tilde{h}_{\alpha\beta\gamma}(\theta, \varphi)$ are universal functions fixed by conformal symmetry, and $f_{\alpha\beta\gamma}$ is the OPE coefficient. Specifically, we may consider the density operator in the vector representation of

SO(5) (i.e., the Sp(2) antisymmetric rank-2 traceless tensor representation) by inserting the γ-matrices

$$\hat{n}^{V,i}(\theta, \varphi) = \hat{\Psi}^\dagger(\theta, \varphi)\gamma^i\hat{\Psi}(\theta, \varphi). \qquad (14)$$

In the perspective of CFT, this operator receives its lowest contribution from the $\hat{\Phi}$ and its descendants $\hat{n}^V = c_\phi\hat{\phi} + c_{\partial_\mu\phi}\partial_\mu\hat{\phi} + c_{\partial^2\phi}\partial^2\hat{\phi} + \dots$

The normalized two-point function of $\hat{n}^V$ therefore receives its leading order contribution from the 2-pt function of $\hat{\phi}$

$$C^V(\theta_1, \varphi_1; \theta_2, \varphi_2) = C^V(\theta_{12})$$

$$= \frac{\langle 0 | \hat{n}^V(\theta_1, \varphi_1)\hat{n}^V(\theta_2, \varphi_2)|0\rangle}{|\langle 0| \int \frac{\sin\theta\, d\theta\, d\varphi}{4\pi}\hat{n}^V(\theta, \varphi)|\phi\rangle|^2}$$

$$= \langle \hat{\phi}(\vec{e}_1)\hat{\phi}(\vec{e}_2)\rangle_{flat} + \mathcal{O}(R^{-1})$$

$$= (2\sin\frac{\theta_{12}}{2})^{-2\Delta_\phi} + \mathcal{O}(R^{-1}), \qquad (15)$$

where θ_{12} is the angular distance and $\vec{e}_{1,2}$ are the unit vector of the two points, the subleading correction $\mathcal{O}(R^{-1})$ comes from the contribution of the descendant $\partial^\mu\hat{\phi}$ on the nominator. Numerically, we find the finite-size result approaches theoretical expectation as N_{orb} increases (Fig. 6a). At large distance near $\theta_{12} = \pi$, the finite-size result has little discrepancy with the theoretical expectation, while the divergence at small distance is not captured by the finite-size numerical result. From the 2-pt function, we can also extract the scaling dimension of ϕ by taking its value at antipodal points

$$C^V(\pi) = 2^{-2\Delta_\phi} + \mathcal{O}(R^{-1}) \qquad (16)$$

and its spatial integral

$$\int \frac{\sin\theta\, d\theta}{2}C^V(\theta) = \frac{2^{-2\Delta_\phi}}{\Delta - 1} + \mathcal{O}(R^{-2}), \qquad (17)$$

where for the latter the subleading contribution comes from $\partial^2\hat{\phi}$ instead. After a finite-size scaling, we extrapolate that $\Delta_\phi^{(antipodal)} = 0.548$ and $\Delta_\phi^{(integral)} = 0.557$ (Fig. 6b), which are 6% and 5% different from the result from the state-operator correspondence 0.584.

On the other hand, we can extract the OPE coefficients by taking the inner product of $\hat{n}^{\mathrm{V}}(\theta, \varphi)$ with CFT states and integrate out the angular dependence [46]. For details see Appendix C. As an example,

$$f_{\phi\phi J} = \sqrt{\frac{3}{2}} \frac{\int \frac{\sin\theta\, d\theta\, d\varphi}{4\pi} \bar{Y}_{10}(\theta, \varphi) \langle \phi | n^{\mathrm{V}}(\theta, \varphi) | J_{m=0} \rangle}{\int \frac{\sin\theta\, d\theta\, d\varphi}{4\pi} \bar{Y}_{00}(\theta, \varphi) \langle \phi | n^{\mathrm{V}}(\theta, \varphi) | 0 \rangle} + \mathcal{O}(R^{-2}). \quad (18)$$

where the subleading contribution comes from $\partial^2 \hat{\phi}$. Similarly, we calculate several OPE coefficients. After a finite-size scaling (Fig. 6c), the extrapolated values are listed in Table III. Here we use a convention that the two-point correlator of J^μ or $\mathcal{T}^{\mu\nu}$ normalizes to 1, so OPE coefficients $f_{\phi\phi J}$ and $f_{\phi\phi\mathcal{T}}$ can give central charges. For example, the stress tensor central charge $C_\mathcal{T} = (\frac{3\Delta_\phi}{4f_{\phi\phi\mathcal{T}}})^2 \approx 6.561 = 0.8748 \cdot (5C_\mathcal{T}^{\mathrm{free}})$, where $C_\mathcal{T}^{\mathrm{free}} = 1.5$ is the central charge of a free scalar [32].

TABLE III. The extrapolated OPE coefficients.

$f_{\phi\phi T}$	$f_{\phi\phi J}$	$f_{\phi\phi S}$	$f_{\phi\phi\mathcal{T}}$
1.242	0.771	0.235	0.121

IV. SUMMARY AND DISCUSSIONS

In this paper, we utilize the fuzzy sphere regularization as a microscope to investigate the SO(5) NLσM with a level-1 WZW term, which serves as one of the dual descriptions of the SO(5) DQCP. We present compelling evidence supporting the presence of an approximate conformal symmetry in the model. Specifically, in the excitation spectrum, we have identified many characteristic features pointing to the SO(5) DQCP, including the conserved SO(5) symmetry current, the stress tensor, and observed integer-spaced levels between primary operators and their descendants. Furthermore, through an examination of the RG flow and the scaling dimension of the parity even SO(5) singlet, we provide support for the scenario that SO(5) DQCP is more likely of a pseudo-critical nature. Additionally, we identify various primary operators, including a relevant 6π-monopole (in the context of the CP^1 model), an irrelevant 8π-monopole, and a highly irrelevant parity odd SO(5) singlet. These findings hold important physical implications. Furthermore, we have computed several OPE coefficients, including the central charge of the stress tensor.

So far, our exploration has been limited to the pseudo-critical phenomenon, which serves as a shadow of the complex fixed point in the complex plane. It is highly intriguing to directly investigate the physics of the complex fixed point itself. Establishing its existence and comprehending its nature would not only conclusively settle the two-decade-long debate surrounding the DQCP but also provide fresh insights into the landscape of fixed points and CFTs, which hold fundamental significance. It is conjectured that the complex fixed point is a relatively common feature in many models and theories, representing one of the few, if not the only, known mechanisms for interaction-driven first-order phase transitions. However, apart from a few examples in 2D (i.e., $(1+1)$D), no example in 3D or higher dimensions has been firmly established thus far. The study of the complex fixed point necessitates the examination of a non-Hermitian Hamiltonian, a task made feasible through the fuzzy sphere technique.

We also emphasize that the observation of pseudo-critical behavior in the DQCP should not diminish its significance. Pseudo-criticality closely resembles true criticality over a wide range of length scales (e.g., system size) or energy scales (e.g., temperature). For instance, any experimental realization of a quantum phase transition is necessarily conducted at a finite temperature, so for a pseudo-critical system one would also observe universal phenomena governed by the complex fixed point. Therefore, employing the fuzzy sphere technique to uncover the CFT perspective of the DQCP at finite temperature, an aspect inaccessible through traditional lattice model simulations, holds great intrigue.

In addition to observing pseudo-critical behavior, we have demonstrated the efficacy of the fuzzy sphere microscope by computing the scaling dimensions of many primary operators. These results play a vital role in enhancing our understanding of the DQCP in various systems, which were previously unattainable through earlier studies. For instance, our findings indicate that the SO(5) DQCP cannot be applied to the Neel-VBS transition on the honeycomb lattice. Consequently, it becomes imperative to employ the fuzzy sphere microscope in investigating other intricate CFTs. One primary target of interest is the U(1) Dirac spin liquid [68–70], whose comprehension holds significant value for experimental studies involving real materials. Specifically, it is crucial to determine the (ir)relevance of specific operators, as this determines whether the U(1) Dirac spin liquid represents a stable phase of matter or a phase transition on triangular or kagome lattices and related materials [71–73].

Another exciting application of the fuzzy sphere microscope is to solve the conformal window problem of 3D critical gauge theories, a long-standing open problem that is interesting to both condensed matter and high-energy physics. Specifically, the SO(5) DQCP studied here is dual to $N = 2$ Dirac fermions coupled to an SU(2) gauge field. We have also provided a simple model for its large-N generalization, which corresponds to the QCD$_3$ theory with $2N$ Dirac fermions coupled to an SU(2) gauge field. By studying this model on the fuzzy sphere, one should be able to determine the precise region of the conformal window (i.e., $N > N_c$) for which the QCD$_3$ theory becomes conformal. The traditional methods, such as lattice model simulations, may not be able to complete this task due to the challenge of distinguishing a true critical (conformal) theory from a pseudo-critical theory. Moreover, generalizing this scheme to other critical gauge theories with different gauge groups should be feasible and interesting to explore in the future.

ACKNOWLEDGMENTS

Appendix A: Sectionning the Hilbert space

In the exact algorithm, we consider the following $U(1)$ conserved quantities

$$\hat{m}^z = \sum_m m\hat{\mathbf{c}}_m^\dagger \hat{\mathbf{c}}_m, \quad \hat{\sigma}_1 = \sum_m \hat{\mathbf{c}}_m^\dagger \sigma_1 \hat{\mathbf{c}}_m, \quad \hat{\sigma}_2 = \sum_m \hat{\mathbf{c}}_m^\dagger \sigma_2 \hat{\mathbf{c}}_m \tag{A1}$$

where

$$\sigma^1 = \begin{pmatrix} 1 & 0 & 0 & 0 \\ 0 & 0 & 0 & 0 \\ 0 & 0 & -1 & 0 \\ 0 & 0 & 0 & 0 \end{pmatrix} \text{ and } \sigma^2 = \begin{pmatrix} 0 & 0 & 0 & 0 \\ 0 & 1 & 0 & 0 \\ 0 & 0 & 0 & 0 \\ 0 & 0 & 0 & -1 \end{pmatrix}.$$

These quantities are conserved because of the SO(3) rotation symmetry and the SO(5) flavor symmetry. These quantities divide the many-body Hilbert space into sectors and block-diagonalize the Hamiltonian. The eigenstates we obtain are also simultaneously eigenstates of these quantities. Using the branching rule $\mathfrak{so}(5) \supset \mathfrak{su}(2) \oplus \mathfrak{su}(2)$ ($\hat{\sigma}^{1,2}$ corresponds to the Cartan subalgebra of the $\mathfrak{su}(2)$s), we can list the degeneracy within each (σ_1, σ_2) sector for each representation (Table IV). By matching the degeneracy of the measured state, we can infer the representation of the corresponding operator.

Appendix B: Full spectrum

In Table V, we list the scaling dimensions of various operators at different V/U and system size N_{orb}. These results support the emergence of approximate conformal symmetry in a vast region $V/U \geq 0.7$.

We list the operator spectrum of operators with $\ell \leq 3$ and $\Delta < 5.5$ measured at $N_{\text{orb}} = 8$ and $V/U = 0.8904$ in Table VI, containing 2691 states corresponding to 137 operators, organized into different representations and conformal multiplets.

Appendix C: OPE tensor structure

The OPE coefficients are defined by the 2-pt and 3-pt functions, namely

$$\langle \phi_i(x_1)\phi_j(x_2)\rangle = \delta_{ij}x_{12}^{-2\tau_\phi}$$
$$\langle T_{ij}(x_1)T_{kl}(x_2)\rangle = T_{ij,kl}x_{12}^{-2\tau_T}$$
$$\langle \hat{J}_{ij}(x_1,z_1)\hat{J}_{kl}(x_2,z_2)\rangle = A_{ij,kl}H(x_1,x_2,z_1,z_2)x_{12}^{-2\tau_J}$$
$$\langle S(x_1)S(x_2)\rangle = x_{12}^{-2\tau_S}$$
$$\langle \hat{\mathscr{T}}(x_1,z_1)\hat{\mathscr{T}}(x_2,z_2)\rangle = H(x_1,x_2,z_1,z_2)^2 x_{12}^{-2\tau_{\mathscr{T}}} \tag{C1}$$

$$\langle \phi_i(x_1)\phi_j(x_2)T_{kl}(x_3)\rangle = \frac{f_{\phi\phi T}T_{ij,kl}}{x_{12}^{2\tau_\phi-\tau_T}x_{23}^{\tau_T}x_{31}^{\tau_T}}$$
$$\langle \phi_i(x_1)\phi_j(x_2)\hat{J}_{kl}(x_3,z_3)\rangle = \frac{f_{\phi\phi J}A_{ij,kl}V(x_1,x_2,x_3,z_3)}{x_{12}^{2\tau_\phi-\tau_J}x_{23}^{\tau_J}x_{31}^{\tau_J}}$$
$$\langle \phi_i(x_1)\phi_j(x_2)S(x_3)\rangle = \frac{f_{\phi\phi S}\delta_{ij}}{x_{12}^{2\tau_\phi-\tau_S}x_{23}^{\tau_S}x_{31}^{\tau_S}}$$
$$\langle \phi_i(x_1)\phi_j(x_2)\hat{\mathscr{T}}(x_3,z_3)\rangle = \frac{f_{\phi\phi\mathscr{T}}\delta_{ij}V(x_1,x_2,x_3,z_3)^2}{x_{12}^{2\tau_\phi-\tau_{\mathscr{T}}}x_{23}^{\tau_{\mathscr{T}}}x_{31}^{\tau_{\mathscr{T}}}}, \tag{C2}$$

where $\tau_\Phi = \Delta_\Phi + \ell_\Phi$; the indices i,j,k,l are SO(5) indices and the tensor structures are given by

$$A_{ij,kl} = \frac{1}{2}\delta_{ik}\delta_{jl} - \frac{1}{2}\delta_{il}\delta_{jk}$$
$$T_{ij,kl} = \frac{1}{2}\delta_{ik}\delta_{jl} + \frac{1}{2}\delta_{il}\delta_{jk} - \frac{1}{5}\delta_{ij}\delta_{kl}. \tag{C3}$$

The Lorentz indices are treated in the index-free treatment where spinning operators are contracted with null auxiliary vector fields

$$\hat{\Phi}_\ell(x,z) = \Phi^{\mu_1\cdots\mu_\ell}(x)z_{\mu_1}\cdots z_{\mu_\ell}, \quad z^2 = 0 \tag{C4}$$

and the Lorentz indices can be recovered by applying the stripping operator

$$D_{z,\mu} = \frac{d-2}{2}\partial_{z_\mu} - z_\nu\partial_{z_\mu}\partial_{z_\nu} - \frac{1}{2}z_\mu\partial_{z_\nu}\partial_{z_\nu}. \tag{C5}$$

The conformal invariant tensors are [74]

$$H(x_1,x_2,z_1,z_2) = \frac{1}{2}x_{12}^2(z_1\cdot z_2) - (z_1\cdot x_{12})(z_2\cdot x_{12})$$
$$V(x_1,x_2,x_3,z_3) = \frac{1}{x_{12}^2}\left[x_{23}^2(z_3\cdot x_{13}) - x_{13}^2(z_3\cdot x_{23})\right]. \tag{C6}$$

We now want to rewrite the correlators in terms of the inner products of states. Consider a spin-ℓ operator $\Phi_{\ell,R}$ in the R-representation of SO(5). Let

$$|\Phi_{\mathbf{n}}^{\mathbf{e}}\rangle = \alpha(\Phi_{\mathbf{n}}^{\mathbf{e}})\lim_{x\to 0} n^{\mu_1\cdots\mu_\ell}e_{ij\ldots}\Phi_{\mu_1\cdots\mu_\ell}^{ij\ldots}(x)|0\rangle, \tag{C7}$$

where $n^{\mu_1\cdots\mu_\ell}$ is the Lorentz polarization, and $e_{ij\ldots}$ is the SO(5) polarization. The coefficient $\alpha(\Phi_{\mathbf{n}}^{\mathbf{e}})$ is determined by the normalisation condition

TABLE IV. The Young diagrams and quadratic Casimir C_2 of different Sp(2) and SO(5) representations and the corresponding state degeneracies in different (σ_1, σ_2) sectors.

rep.	Young diagram Sp(2)	SO(5)	C_2	Degeneracy $(0,0)$	$(1,1)$	$(2,0)$	$(2,2)$	$(3,1)$	$(3,3)$	$(4,0)$	$(4,2)$	$(4,4)$
1			0	1								
5			2	1	1							
10			3	2	1	1						
14			5	2	1	1	1					
30			9	2	2	1	1	1	1			
35			6	3	3	2	1	1				
35′			8	3	2	2	1	1		1		
55			14	3	2	2	2	1	1	1	1	1

TABLE V. The scaling dimensions of several operators at different V/U and system size $N_{\rm orb}$ calibrated by the scaling dimension of the symmetry current $\Delta_J = 2$. The quantum numbers $(\ell, \mathscr{P}, \text{rep.})$ are given in the bracket. (a) the conserved stress tensor $\mathscr{T}^{\mu\nu}$, fixed to be 3 by conformal symmetry; (b) the difference of scaling dimension of ϕ and its descendant $\partial^\mu\phi$, fixed to be 1 by conformal symmetry; (c) the difference of scaling dimension of ϕ and its descendant $\partial^\mu\partial^\nu\phi$, fixed to be 2 by conformal symmetry; (d) the descendant $\epsilon^{\mu\nu\rho}\partial_\nu J_\rho$ of the conserved current J^μ, fixed to be 3 by conformal symmetry; (e) the descendant $\partial^\mu J^\nu$ of the conserved current J^μ, fixed to be 3 by conformal symmetry; (f) the difference of scaling dimension of T and its descendant $\partial^\mu T$, fixed to be 1 by conformal symmetry. The empty entries are beyond our calculation capacity.

V/U	$N_{\rm orb}$ — a. $\mathscr{T}^{\mu\nu}$, $(2,+,\mathbf{1})$					b. $\partial^\mu\phi$, $(2,-,\mathbf{5})-\phi$					c. $\partial^\mu\partial^\nu\phi$, $(1,-,\mathbf{5})-\phi$				
	9	8	7	6	5	9	8	7	6	5	9	8	7	6	5
0.300	3.413	3.427	3.452	3.493	3.565	1.399	1.395	1.393	1.392	1.393	2.856	2.833	2.803	2.760	2.695
0.700	3.080	3.079	3.079	3.086	3.103	1.151	1.149	1.146	1.143	1.139	2.178	2.155	2.126	2.086	2.030
0.915	3.000	2.992	2.983	2.976	2.973	1.097	1.093	1.089	1.083	1.076	2.022	1.995	1.961	1.916	1.855
1.011	2.973	2.962	2.950	2.938	2.928	1.080	1.076	1.070	1.063	1.055	1.971	1.942	1.906	1.859	1.796
1.500	2.880	2.859	2.834	2.802	2.764	1.027	1.020	1.011	0.999	0.984	1.806	1.768	1.723	1.665	1.590
3.000	2.758	2.720	2.674	2.615	2.539	0.974	0.962	0.947	0.928	0.902	1.618	1.568	1.506	1.431	1.337
10.00	2.634	2.579	2.511	2.427	2.321	0.938	0.921	0.901	0.874	0.839	1.471	1.408	1.332	1.239	1.125

V/U	d. $\epsilon^{\mu\nu\rho}\partial_\nu J_\rho$, $(1,-,\mathbf{10})$					e. $\partial^\mu J^\nu$, $(2,+,\mathbf{10})$					f. $\partial^\mu T$, $(1,+,\mathbf{14})-T$				
	9	8	7	6	5	9	8	7	6	5	9	8	7	6	5
0.300		3.270	3.241	3.206	3.161		3.432	3.396	3.343	3.263	1.389	1.383	1.378	1.373	1.369
0.700	3.093	3.084	3.074	3.060	3.041	3.016	2.995	2.967	2.927	2.870	1.139	1.132	1.123	1.111	1.096
0.915	3.057	3.051	3.043	3.033	3.018	2.922	2.899	2.870	2.829	2.772	1.079	1.070	1.059	1.044	1.023
1.011	3.047	3.041	3.034	3.025	3.011	2.892	2.869	2.838	2.797	2.739	1.060	1.050	1.037	1.021	0.998
1.500	3.016	3.012	3.006	2.999	2.988	2.798	2.770	2.735	2.690	2.630	0.996	0.982	0.965	0.942	0.910
3.000	2.985	2.980	2.975	2.968	2.959	2.696	2.661	2.619	2.566	2.499	0.923	0.903	0.878	0.846	0.802
10.00		2.950	2.944	2.936	2.928		2.577	2.527	2.467	2.393		0.840	0.808	0.766	0.710

TABLE VI. The full low lying states with $\ell \leq 3$ and $\Delta < 5.5$ measured at $N_{\mathrm{orb}} = 8$ and $V/U = 0.8904$, organized into different representations and conformal multiplets. The "P" and "D" in the last column denote the identified primaries and their descendants. The short dash divides multiplets and the line divides representations.

ℓ	$\mathscr{P}$	rep.	Δ		ℓ	$\mathscr{P}$	rep.	Δ		ℓ	$\mathscr{P}$	rep.	Δ		ℓ	$\mathscr{P}$	rep.	Δ	
0	+	1	0.0000		1	+	5	5.0688	D	0	+	14	1.4522	P	1	−	35	5.0982	D
0	+	1	2.8654	P	3	−	5	4.6158		1	+	14	2.5282	D	1	−	35	5.2452	D
1	+	1	3.9531	D	0	−	5	5.0742		2	+	14	3.3953	D	2	−	35	3.5437	P
2	+	1	4.6855	D	3	−	5	5.0969		0	+	14	3.7839	D	1	−	35	4.4528	D
0	+	1	5.1220	D	1	−	5	5.1397		3	+	14	4.1018	D	3	−	35	4.4881	D
3	+	1	5.3837	D	3	−	5	5.4088		1	+	14	4.6794	D	2	+	35	4.5096	D
2	+	1	3.0000	P	1	+	10	2.0000	P	2	+	14	5.4343	D	2	−	35	5.3949	D
3	+	1	3.7932	D	2	+	10	2.9081	D	2	+	14	3.3254	P	1	+	35	5.4764	D
2	−	1	4.0107	D	1	−	10	3.0541	D	3	+	14	3.9311	D	3	+	35	5.4928	D
3	−	1	4.5941	D	3	+	10	3.5263	D	2	−	14	4.3379	D	3	−	35	4.2530	P
2	+	1	4.9309	D	2	−	10	3.8536	D	1	+	14	4.7298	D	2	−	35	5.2503	D
3	+	1	5.0764		1	+	10	4.0818	D	2	+	14	5.1951	D	3	+	35	5.2776	D
2	+	1	4.8959		3	−	10	4.4248	D	2	+	14	5.3692	D	1	−	35	4.7506	
0	−	1	5.3659		2	+	10	4.7951	D	3	−	14	5.4479	D	2	−	35	4.7772	
0	−	5	0.5828	P	1	−	10	5.0482	D	0	+	14	4.3846	P	2	+	35	4.7878	
1	−	5	1.6813	D	1	+	10	3.1710	P	1	+	14	5.3445	D	1	+	35	4.8614	
2	−	5	2.5928	D	2	+	10	4.0300	D	2	+	14	4.8785		3	+	35	5.0694	
0	−	5	2.9729	D	1	−	10	4.2397	D	3	−	14	4.9226		3	+	35	5.3028	
3	−	5	3.2166	D	0	+	10	4.3181	D	2	−	14	5.2915		3	−	35	5.4472	
1	−	5	3.9487	D	3	+	10	4.5795	D	2	+	14	5.4870		0	+	35′	4.9206	
0	−	5	4.3624	D	2	−	10	5.0237	D	0	−	30	2.5623	P	2	+	35′	4.6691	
2	−	5	4.6656	D	1	+	10	5.2088	D	1	−	30	3.5948	D	2	−	35′	5.1619	
1	−	5	5.3446	D	1	+	10	5.2259	D	2	−	30	4.4735	D	3	+	35′	5.3495	
3	−	5	5.3479	D	3	+	10	4.1976	P	0	−	30	4.8108	D	0	+	55	3.8812	P
2	−	5	3.8456	P	3	−	10	5.0642	D	3	−	30	5.1747	D	1	+	55	4.8532	D
1	−	5	4.5357	D	2	+	10	5.3673	D	2	−	30	4.3519	P	1	+	81	4.2866	P
3	−	5	4.5698	D	3	−	10	4.3484	P	3	−	30	5.0239	D	2	+	81	5.1193	D
2	+	5	4.8400	D	3	+	10	5.4692	D	2	+	30	5.3684	D	1	−	81	5.3061	D
2	−	5	5.3723	D	1	+	10	4.5389		3	−	30	4.8667		2	+	81	4.7750	
3	+	5	5.3837	D	2	−	10	4.8752		1	−	35	3.0275	P	3	+	81	5.1311	
2	−	5	5.4854	D	3	+	10	5.1489		2	−	35	3.9105	D	3	+	81	5.4517	
3	+	5	5.4872	D	1	−	10	5.1701		1	+	35	4.0875	D	0	−	91	5.3845	
2	+	5	3.9725	P	3	+	10	5.2175		0	−	35	4.2917	D					
3	+	5	4.6463	D	3	+	10	5.3128		2	+	35	4.8634	D					
2	−	5	4.8686	D	3	−	10	5.4004		3	−	35	4.9814	D					

$$\langle \Phi_{\mathbf{n}}^{\mathbf{e}} | \Phi_{\mathbf{n}}^{\mathbf{e}} \rangle = |\alpha(\Phi_{\mathbf{n}}^{\mathbf{e}})|^2 \lim_{x \to 0} (n^*)^{\mu_1' \dots \mu_\ell'} n^{\mu_1 \dots \mu_\ell} e^*_{i'j'\dots} e_{ij\dots} \langle (\Phi_{\mu_1' \dots \mu_\ell'}^{i'j'\dots}(x))^\dagger \Phi_{\mu_1 \dots \mu_\ell}^{ij\dots}(x) \rangle, \tag{C8}$$

where the conjugation in the radial quantization is taken as

$$(\Phi^\dagger)_{\mu_1 \dots \mu_\ell}^{ij\dots}(x) = x^{2\Delta} I_{\mu_1}{}^{\nu_1}(x) \dots I_{\mu_\ell}{}^{\nu_\ell}(x) \Phi_{\nu_1 \dots \nu_\ell}^{ij\dots}\left(\frac{x^\mu}{x^2}\right), \tag{C9}$$

where $I_\mu{}^\nu(x) = \delta_\mu^\nu - 2x_\mu x^\nu / x^2$. Hence,

$$\alpha(\Phi_{\mathbf{n}}^{\mathbf{e}}) = \left[\lim_{x \to \infty} x^{2\Delta_\Phi} (n^*)^{\mu_1' \dots \mu_\ell'} n^{\mu_1 \dots \mu_\ell} e^*_{i'j'\dots} e_{ij\dots} I_{\mu_1'}{}^{\nu_1}(x) \dots I_{\mu_\ell'}{}^{\nu_\ell}(x) \langle \Phi_{\nu_1 \dots \nu_\ell}^{i'j'\dots}(x) \Phi_{\mu_1 \dots \mu_\ell}^{ij\dots}(0) \rangle \right]^{-1/2}. \tag{C10}$$

Specifically, for the Lorentz polarization, we consider eigenstates of $\hat{L}^2$ and $\hat{L}^z$ labeled by l and m and pick out $m = 0$ components. For $\ell \leq 2$, the non-zero components of the polarizations are chosen as

$$n_{(l,m)=(0,0)} = 1$$
$$n_{(l,m)=(1,0)}^z = 1$$
$$n_{(l,m)=(2,0)}^{zz} = 2 \quad n_{(l,m)=(2,0)}^{xx} = n_{(l,m)=(2,0)}^{yy} = -1. \tag{C11}$$

For the SO(5) polarization, we consider eigenstates of $\hat{\sigma}_1$ and $\hat{\sigma}_2$. The basis of γ-matrices are taken as

$$\gamma^{1,\dots,5} = \{\mathbb{I} \otimes \tau^x, \mathbb{I} \otimes \tau^z, \sigma^x \otimes \tau^y, \sigma^y \otimes \tau^y, \sigma^z \otimes \tau^y\}, \tag{C12}$$

and the polarizations are determined by

$$[e_{ij\dots}^{(\sigma_1,\sigma_2)} \gamma^i \otimes \gamma^j \otimes \dots, \hat{\sigma}^\alpha] = \sigma^\alpha e_{ij\dots}^{(\sigma_1,\sigma_2)} \gamma^i \otimes \gamma^j \otimes \dots, \tag{C13}$$

where $\alpha = 1, 2$. We pick out the $(\sigma_1, \sigma_2) = (0,0), (1,1)$ components of the vector representation and the $(\sigma_1, \sigma_2) = (1,1)$ components of the symmetric and antisymmetric rank-2 tensor representations. The non-zero components of the polarizations are chosen as

$$e^{S,(\sigma_1,\sigma_2)=(0,0)} = 1$$
$$e_2^{V,(\sigma_1,\sigma_2)=(0,0)} = 1$$
$$e_4^{V,(\sigma_1,\sigma_2)=(1,1)} = 1/\sqrt{2} \quad e_3^{V,(\sigma_1,\sigma_2)=(1,1)} = -i/\sqrt{2}$$
$$e_{24}^{A,(\sigma_1,\sigma_2)=(1,1)} = 1/\sqrt{2} \quad e_{23}^{A,(\sigma_1,\sigma_2)=(1,1)} = -i/\sqrt{2}$$
$$e_{24}^{T,(\sigma_1,\sigma_2)=(1,1)} = 1/\sqrt{2} \quad e_{23}^{T,(\sigma_1,\sigma_2)=(1,1)} = -i/\sqrt{2}. \tag{C14}$$

Hence, the normalizing factors are taken as

$$\alpha(S_{(l,m)=(0,0)}^{(\sigma_1,\sigma_2)=(0,0)}) = 1 \quad \alpha(\phi_{(l,m)=(0,0)}^{(\sigma_1,\sigma_2)=(0,0)}) = 1$$
$$\alpha(\phi_{(l,m)=(0,0)}^{(\sigma_1,\sigma_2)=(1,1)}) = 1 \quad \alpha(T_{(l,m)=(0,0)}^{(\sigma_1,\sigma_2)=(1,1)}) = \sqrt{2}$$
$$\alpha(J_{(l,m)=(1,0)}^{(\sigma_1,\sigma_2)=(1,1)}) = 4 \quad \alpha(\mathscr{T}_{(l,m)=(2,0)}^{(\sigma_1,\sigma_2)=(0,0)}) = \sqrt{8/27}. \tag{C15}$$

With this, the 3-pt functions in general can be written as

$$\langle (\Phi_1)_{\mathbf{n_1}}^{\mathbf{e_1}} | (\Phi_2)_{\mathbf{n_2}}^{\mathbf{e_2}}(\theta, \varphi) | (\Phi_3)_{\mathbf{n_3}}^{\mathbf{e_3}} \rangle = \alpha^*((\Phi_1)_{\mathbf{n_1}}^{\mathbf{e_1}}) \alpha((\Phi_3)_{\mathbf{n_3}}^{\mathbf{e_3}}) \lim_{x \to \infty} x^{2\Delta_1} (n_1^*)^{\mu_1'' \dots \mu_\ell''} n_2^{\mu_1' \dots \mu_\ell'} n_3^{\mu_1 \dots \mu_\ell} e^*_{1,i''j''\dots} e_{2,i'j'\dots} e_{3,ij\dots}$$
$$\times I_{\mu_1''}{}^{\nu_1}(x) \dots I_{\mu_\ell''}{}^{\nu_\ell}(x) \left\langle (\Phi_1)_{\nu_1 \dots \nu_\ell}^{i''j''\dots}(x) (\Phi_2)_{\mu_1' \dots \mu_\ell'}^{i'j'\dots}(\theta, \varphi)(\Phi_3)_{\mu_1 \dots \mu_\ell}^{ij\dots}(0) \right\rangle. \tag{C16}$$

Specifically

$$\langle \phi_{(l,m)=(0,0)}^{(\sigma_1,\sigma_2)=(0,0)} | \phi^{(\sigma_1,\sigma_2)=(0,0)}(\theta, \varphi) | S_{(l,m)=(0,0)}^{(\sigma_1,\sigma_2)=(0,0)} \rangle = R^{-\Delta_\phi} f_{\phi\phi S}$$
$$\langle \phi_{(l,m)=(0,0)}^{(\sigma_1,\sigma_2)=(1,1)} | \phi^{(\sigma_1,\sigma_2)=(0,0)}(\theta, \varphi) | J_{(l,m)=(1,0)}^{(\sigma_1,\sigma_2)=(1,1)} \rangle = R^{-\Delta_\phi} f_{\phi\phi J} \cos\theta$$
$$\langle \phi_{(l,m)=(0,0)}^{(\sigma_1,\sigma_2)=(1,1)} | \phi^{(\sigma_1,\sigma_2)=(0,0)}(\theta, \varphi) | T_{(l,m)=(0,0)}^{(\sigma_1,\sigma_2)=(1,1)} \rangle = \frac{1}{\sqrt{2}} R^{-\Delta_\phi} f_{\phi\phi T}$$
$$\langle \phi_{(l,m)=(0,0)}^{(\sigma_1,\sigma_2)=(0,0)} | \phi^{(\sigma_1,\sigma_2)=(0,0)}(\theta, \varphi) | \mathscr{T}_{(l,m)=(2,0)}^{(\sigma_1,\sigma_2)=(0,0)} \rangle = \frac{1}{\sqrt{6}} R^{-\Delta_\phi} f_{\phi\phi\mathscr{T}}(1 + 3\cos 2\theta). \tag{C17}$$

We then integrate out the angular dependence by taking the angular momentum component

$$\hat{\phi}_{lm} = \int \frac{\sin\theta \, d\theta \, d\varphi}{4\pi} \bar{Y}_{lm}(\theta,\varphi) \hat{\phi}(\theta,\varphi). \tag{C18}$$

In our calculation, we use the density operator $\hat{n}$ instead of $\hat{\phi}$. To the leading order

$$\hat{n}(\theta,\varphi) = \alpha_\phi \hat{\phi} + \dots \tag{C19}$$

and the coefficient can be accessed by

$$\langle \phi | \hat{n}(\theta,\varphi) | 0 \rangle = \alpha_\phi R^{-\Delta_\phi} (1 + \mathcal{O}(R^{-2})). \tag{C20}$$

The subleading contribution comes from the descendants of ϕ and other multiplets in the same sector.

Hence, to the leading order

$$f_{\phi\phi S} = \frac{\langle \phi^{(\sigma_1,\sigma_2)=(0,0)}_{(l,m)=(0,0)} | n^{(\sigma_1,\sigma_2)=(0,0)}_{(l,m)=(0,0)} | S^{(\sigma_1,\sigma_2)=(0,0)}_{(l,m)=(0,0)} \rangle}{\langle \phi^{(\sigma_1,\sigma_2)=(0,0)}_{(l,m)=(0,0)} | n^{(\sigma_1,\sigma_2)=(0,0)}_{(l,m)=(0,0)} | 0 \rangle}$$

$$f_{\phi\phi J} = \sqrt{3} \frac{\langle \phi^{(\sigma_1,\sigma_2)=(1,1)}_{(l,m)=(0,0)} | n^{(\sigma_1,\sigma_2)=(0,0)}_{(l,m)=(1,0)} | J^{(\sigma_1,\sigma_2)=(1,1)}_{(l,m)=(1,0)} \rangle}{\langle \phi^{(\sigma_1,\sigma_2)=(0,0)}_{(l,m)=(0,0)} | n^{(\sigma_1,\sigma_2)=(0,0)}_{(l,m)=(0,0)} | 0 \rangle}$$

$$f_{\phi\phi T} = \sqrt{2} \frac{\langle \phi^{(\sigma_1,\sigma_2)=(1,1)}_{(l,m)=(0,0)} | n^{(\sigma_1,\sigma_2)=(0,0)}_{(l,m)=(0,0)} | T^{(\sigma_1,\sigma_2)=(1,1)}_{(l,m)=(0,0)} \rangle}{\langle \phi^{(\sigma_1,\sigma_2)=(0,0)}_{(l,m)=(0,0)} | n^{(\sigma_1,\sigma_2)=(0,0)}_{(l,m)=(0,0)} | 0 \rangle}$$

$$f_{\phi\phi\mathscr{T}} = \sqrt{\frac{15}{8}} \frac{\langle \phi^{(\sigma_1,\sigma_2)=(0,0)}_{(l,m)=(0,0)} | n^{(\sigma_1,\sigma_2)=(0,0)}_{(l,m)=(2,0)} | \mathscr{T}^{(\sigma_1,\sigma_2)=(0,0)}_{(l,m)=(2,0)} \rangle}{\langle \phi^{(\sigma_1,\sigma_2)=(0,0)}_{(l,m)=(0,0)} | n^{(\sigma_1,\sigma_2)=(0,0)}_{(l,m)=(0,0)} | 0 \rangle}.$$

$$\tag{C21}$$

[1] S. Sachdev, *Quantum Phase Transitions*, 2nd ed. (Cambridge University Press, 2011).

[2] T. Senthil, A. Vishwanath, L. Balents, S. Sachdev, and M. P. A. Fisher, Deconfined quantum critical points, Science **303**, 1490 (2004).

[3] T. Senthil, L. Balents, S. Sachdev, A. Vishwanath, and M. P. A. Fisher, Quantum criticality beyond the Landau-Ginzburg-Wilson paradigm, Phys. Rev. B **70**, 144407 (2004).

[4] N. Read and S. Sachdev, Spin-Peierls, valence-bond solid, and Néel ground states of low-dimensional quantum antiferromagnets, Phys. Rev. B **42**, 4568 (1990).

[5] N. Read and S. Sachdev, Valence-bond and spin-Peierls ground states of low-dimensional quantum antiferromagnets, Phys. Rev. Lett. **62**, 1694 (1989).

[6] G. Murthy and S. Sachdev, Action of hedgehog instantons in the disordered phase of the $(2+1)$-dimensional CP^{N-1} model, Nucl. Phys. B **344**, 557 (1990).

[7] A. Nahum, P. Serna, J. T. Chalker, M. Ortuño, and A. M. Somoza, Emergent SO(5) symmetry at the Néel to valence-bond-solid transition, Phys. Rev. Lett. **115**, 267203 (2015).

[8] C. Wang, A. Nahum, M. A. Metlitski, C. Xu, and T. Senthil, Deconfined quantum critical points: Symmetries and dualities, Phys. Rev. X **7**, 031051 (2017).

[9] O. I. Motrunich and A. Vishwanath, Emergent photons and transitions in the O(3) sigma model with hedgehog suppression, Phys. Rev. B **70**, 075104 (2004).

[10] A. W. Sandvik, Evidence for deconfined quantum criticality in a two-dimensional Heisenberg model with four-spin interactions, Phys. Rev. Lett. **98**, 227202 (2007).

[11] R. G. Melko and R. K. Kaul, Scaling in the fan of an unconventional quantum critical point, Phys. Rev. Lett. **100**, 017203 (2008).

[12] F. J. Jiang, M. Nyfeler, S. Chandrasekharan, and U. J. Wiese, From an antiferromagnet to a valence bond solid: evidence for a first-order phase transition, J. Stat. Mech. **2008**, 02009 (2008).

[13] A. B. Kuklov, M. Matsumoto, N. V. Prokof'ev, B. V. Svistunov, and M. Troyer, Deconfined criticality: Generic first-order transition in the SU(2) symmetry case, Phys. Rev. Lett. **101**, 050405 (2008).

[14] A. W. Sandvik, Continuous quantum phase transition between an antiferromagnet and a valence-bond solid in two dimensions: Evidence for logarithmic corrections to scaling, Phys. Rev. Lett. **104**, 177201 (2010).

[15] J. Lou, A. W. Sandvik, and N. Kawashima, Antiferromagnetic to valence-bond-solid transitions in two-dimensional SU(N) Heisenberg models with multispin interactions, Phys. Rev. B **80**, 180414 (2009).

[16] A. Banerjee, K. Damle, and F. Alet, Impurity spin texture at a deconfined quantum critical point, Phys. Rev. B **82**, 155139 (2010).

[17] R. K. Kaul and A. W. Sandvik, Lattice model for the SU(N) Néel to valence-bond solid quantum phase transition at large N, Phys. Rev. Lett. **108**, 137201 (2012).

[18] R. K. Kaul, Quantum phase transitions in bilayer SU(N) antiferromagnets, Phys. Rev. B **85**, 180411 (2012).

[19] L. Bartosch, Corrections to scaling in the critical theory of deconfined criticality, Phys. Rev. B **88**, 195140 (2013).

[20] K. Chen, Y. Huang, Y. Deng, A. B. Kuklov, N. V. Prokof'ev, and B. V. Svistunov, Deconfined criticality flow in the Heisenberg model with ring-exchange interactions, Phys. Rev. Lett. **110**, 185701 (2013).

[21] S. Pujari, K. Damle, and F. Alet, Néel-state to valence-bond-solid transition on the honeycomb lattice: Evidence for deconfined criticality, Phys. Rev. Lett. **111**, 087203 (2013).

[22] A. Nahum, J. T. Chalker, P. Serna, M. Ortuño, and A. M. Somoza, Deconfined quantum criticality, scaling violations, and classical loop models, Phys. Rev. X **5**, 041048 (2015).

[23] G. J. Sreejith and S. Powell, Scaling dimensions of higher-charge monopoles at deconfined critical points, Phys. Rev. B **92**, 184413 (2015).

[24] G. J. Sreejith and S. Powell, Critical behavior in the cubic dimer model at nonzero monomer density, Phys. Rev. B **89**, 014404 (2014).

[25] H. Shao, W. Guo, and A. W. Sandvik, Quantum criticality with two length scales, Science **352**, 213 (2016).

[26] T. Sato, M. Hohenadler, and F. F. Assaad, Dirac fermions with competing orders: Non-Landau transition with emergent symmetry, Phys. Rev. Lett. **119**, 197203 (2017).

[27] P. Serna and A. Nahum, Emergence and spontaneous breaking of approximate O(4) symmetry at a weakly first-order deconfined phase transition, Phys. Rev. B **99**, 195110 (2019).

[28] Y. Liu, Z. Wang, T. Sato, M. Hohenadler, C. Wang, W. Guo, and F. F. Assaad, Superconductivity from the condensation of topological defects in a quantum spin-Hall insulator, Nat. Commun. **10**, 2658 (2019).

[29] B. Zhao, J. Takahashi, and A. W. Sandvik, Multicritical decon-

fined quantum criticality and Lifshitz point of a helical valence-bond phase, Phys. Rev. Lett. **125**, 257204 (2020).

[30] Z. Wang, M. P. Zaletel, R. S. K. Mong, and F. F. Assaad, Phases of the $(2 + 1)$ dimensional SO(5) nonlinear sigma model with topological term, Phys. Rev. Lett. **126**, 045701 (2021).

[31] T. Senthil, Deconfined quantum critical points: a review, arXiv:2306.12638.

[32] D. Poland, S. Rychkov, and A. Vichi, The conformal bootstrap: Theory, numerical techniques, and applications, Rev. Mod. Phys. **91**, 015002 (2019).

[33] Y. Nakayama and T. Ohtsuki, Necessary condition for emergent symmetry from the conformal bootstrap, Phys. Rev. Lett. **117**, 131601 (2016).

[34] V. Gorbenko, S. Rychkov, and B. Zan, Walking, weak first-order transitions, and complex CFTs, J. High Energy Phys. **10** (2018), 108.

[35] V. Gorbenko, S. Rychkov, and B. Zan, Walking, weak first-order transitions, and complex CFTs II. two-dimensional Potts model at $Q > 4$, SciPost Phys. **5**, 050 (2018).

[36] B. Nienhuis, A. N. Berker, E. K. Riedel, and M. Schick, First- and second-order phase transitions in Potts models: Renormalization-group solution, Phys. Rev. Lett. **43**, 737 (1979).

[37] H. Ma and Y.-C. He, Shadow of complex fixed point: Approximate conformality of $Q > 4$ Potts model, Phys. Rev. B **99**, 195130 (2019).

[38] R. Ma and C. Wang, Theory of deconfined pseudocriticality, Phys. Rev. B **102**, 020407 (2020).

[39] A. Nahum, Note on Wess-Zumino-Witten models and quasiuniversality in $2 + 1$ dimensions, Phys. Rev. B **102**, 201116 (2020).

[40] J. D'Emidio, A. A. Eberharter, and A. M. Läuchli, Diagnosing weakly first-order phase transitions by coupling to order parameters, arXiv:2106.15462.

[41] J. Zhao, Y.-C. Wang, Z. Yan, M. Cheng, and Z. Y. Meng, Scaling of entanglement entropy at deconfined quantum criticality, Phys. Rev. Lett. **128**, 010601 (2022).

[42] W. Zhu, C. Han, E. Huffman, J. S. Hofmann, and Y.-C. He, Uncovering conformal symmetry in the 3D Ising transition: State-operator correspondence from a quantum fuzzy sphere regularization, Phys. Rev. X **13**, 021009 (2023).

[43] J. Madore, The fuzzy sphere, Class. Quantum Gravity **9**, 69 (1992).

[44] J. L. Cardy, Conformal invariance and universality in finite-size scaling, J. Phys. A **17**, L385 (1984).

[45] J. L. Cardy, Universal amplitudes in finite-size scaling: generalisation to arbitrary dimensionality, J. Phys. A **18**, L757 (1985).

[46] L. Hu, Y.-C. He, and W. Zhu, Operator product expansion coefficients of the 3D Ising criticality via quantum fuzzy sphere, arXiv:2303.08844.

[47] C. Han, L. Hu, W. Zhu, and Y.-C. He, Conformal four-point correlators of the 3D Ising transition via the quantum fuzzy sphere, arXiv:2306.04681.

[48] M. Ippoliti, R. S. K. Mong, F. F. Assaad, and M. P. Zaletel, Half-filled Landau levels: A continuum and sign-free regularization for three-dimensional quantum critical points, Phys. Rev. B **98**, 235108 (2018).

[49] R. Samajdar, M. S. Scheurer, S. Chatterjee, H. Guo, C. Xu, and S. Sachdev, Enhanced thermal Hall effect in the square-lattice Néel state, Nat. Phys. **15**, 1290 (2019).

[50] The Hamiltonian in Ref. [30, 48] is

$$H_{\text{int}} = \int \mathrm{d}^2\vec{r} \left[\tilde{U}_0 \hat{n}(\vec{r})^2 - \tilde{U}(\hat{\Psi}^\dagger \gamma^i \hat{\Psi})(\vec{r})^2 \right].$$

As $(\hat{\Psi}^\dagger \gamma^i \hat{\Psi})^2 = -(3/4)\hat{n}^2 + (1/2)\hat{\Delta}^\dagger \hat{\Delta}$, it converts into our

Hamiltonian as

$$U(\vec{r}_1, \vec{r}_2) = (\tilde{U}_0 + (3/4)\tilde{U})\delta(\vec{r}_{12}),$$
$$V(\vec{r}_1, \vec{r}_2) = 2\tilde{U}\delta(\vec{r}_{12}).$$

.

[51] J. Lee and S. Sachdev, Wess-Zumino-Witten terms in graphene landau levels, Phys. Rev. Lett. **114**, 226801 (2015).

[52] C. Xu, Three-dimensional symmetry-protected topological phase close to antiferromagnetic néel order, Phys. Rev. B **87**, 144421 (2013).

[53] Z. Komargodski and N. Seiberg, A symmetry breaking scenario for QCD₃, J. High Energy Phys. **01** (2018), 109.

[54] S. L. Sondhi, A. Karlhede, S. A. Kivelson, and E. H. Rezayi, Skyrmions and the crossover from the integer to fractional quantum hall effect at small Zeeman energies, Phys. Rev. B **47**, 16419 (1993).

[55] F. D. M. Haldane, Fractional quantization of the hall effect: A hierarchy of incompressible quantum fluid states, Phys. Rev. Lett. **51**, 605 (1983).

[56] T. T. Wu and C. N. Yang, Dirac monopole without strings: Monopole harmonics, Nucl. Phys. B **107**, 365 (1976).

[57] L. Zou, Y.-C. He, and C. Wang, Stiefel liquids: Possible non-lagrangian quantum criticality from intertwined orders, Phys. Rev. X **11**, 031043 (2021).

[58] C. Xu, Renormalization group studies on four-fermion interaction instabilities on algebraic spin liquids, Phys. Rev. B **78**, 054432 (2008).

[59] D. B. Kaplan, J.-W. Lee, D. T. Son, and M. A. Stephanov, Conformality lost, Phys. Rev. D **80**, 125005 (2009).

[60] The reason for $\Delta_S \gtrsim 3$ at the beginning of the RG flow is that the flow is attractive, leading towards the vicinity of complex fixed points. On the other hand, the complex fixed points themselves have $\mathrm{Re}(\Delta_S) \lesssim 3$, causing Δ_S to eventually become relevant once the system flows in the vicinity of the complex fixed points.

[61] M. Levin and T. Senthil, Deconfined quantum criticality and Néel order via dimer disorder, Phys. Rev. B **70**, 220403 (2004).

[62] A. Tanaka and X. Hu, Many-body spin Berry phases emerging from the π-flux state: Competition between antiferromagnetism and the valence-bond-solid state, Phys. Rev. Lett. **95**, 036402 (2005).

[63] T. Senthil and M. P. A. Fisher, Competing orders, nonlinear sigma models, and topological terms in quantum magnets, Phys. Rev. B **74**, 064405 (2006).

[64] R. Ma, L. Zou, and C. Wang, Edge physics at the deconfined transition between a quantum spin Hall insulator and a superconductor, SciPost Phys. **12**, 196 (2022).

[65] In the CP¹ description, this operator has a large engineer dimension.

[66] A. W. Sandvik and B. Zhao, Consistent scaling exponents at the deconfined quantum-critical point, Chin. Phys. Lett. **37**, 057502 (2020).

[67] T. Grover and T. Senthil, Topological Spin Hall States, Charged Skyrmions, and Superconductivity in Two Dimensions, Phys. Rev. Lett. **100**, 156804 (2008).

[68] I. Affleck and J. B. Marston, Large-n limit of the heisenberg-hubbard model: Implications for high-T_c superconductors, Phys. Rev. B **37**, 3774 (1988).

[69] X.-G. Wen and P. A. Lee, Theory of Underdoped Cuprates, Phys. Rev. Lett. **76**, 503 (1996).

[70] M. Hermele, T. Senthil, and M. P. A. Fisher, Algebraic spin liquid as the mother of many competing orders, Phys. Rev. B **72**, 104404 (2005).

[71] C.-M. Jian, A. Thomson, A. Rasmussen, Z. Bi, and C. Xu,

Deconfined quantum critical point on the triangular lattice, Phys. Rev. B **97**, 195115 (2018).

[72] X.-Y. Song, Y.-C. He, A. Vishwanath, and C. Wang, From spinon band topology to the symmetry quantum numbers of monopoles in Dirac spin liquids, Phys. Rev. X **10**, 011033 (2020).

[73] X.-Y. Song, C. Wang, A. Vishwanath, and Y.-C. He, Unifying description of competing orders in two-dimensional quantum magnets, Nat. Commun. **10**, 4254 (2019).

[74] M. S. Costa, J. Penedones, D. Poland, and S. Rychkov, Spinning conformal correlators, J. High Energy Phys. **11** (2011), 071.